# UCSF

**Title**

RasGRP1 opposes proliferative EGFR–SOS1–Ras signals and restricts intestinal epithelial cell growth

**Authors**

Depeille, Philippe
Henricks, Linda M
van de Ven, Robert AH
et al.

# RasGRP1 opposes proliferative EGFR–SOS1–Ras signals and restricts intestinal epithelial cell growth

**Philippe Depeille**[1,6], **Linda M. Henricks**[1,5], **Robert A. H. van de Ven**[1,5], **Ed Lemmens**[1,5], **Chih-Yang Wang**[1,2], **Mary Matli**[3], **Zena Werb**[1], **Kevin M. Haigis**[4], **David Donner**[3], **Robert Warren**[3], and **Jeroen P. Roose**[1,6]

[1]Department of Anatomy, University of California, San Francisco, San Francisco, California 94143, USA

[2]Institute of Basic Medical Sciences, College of Medicine, National Cheng Kung University, Tainan 70101, Taiwan

[3]Department of Surgery, University of California, San Francisco, San Francisco, California 94143, USA

[4]Molecular Pathology Unit, Massachusetts General Hospital, Charlestown, Massachusetts 02129, USA

## Abstract

The character of EGFR signals can influence cell fate but mechanistic insights into intestinal EGFR-Ras signalling are limited. Here we show that two distinct Ras nucleotide exchange factors, RasGRP1 and SOS1, lie downstream of EGFR but act in functional opposition. RasGRP1 is expressed in intestinal crypts where it restricts epithelial growth. High RasGRP1 expression in colorectal cancer (CRC) patient samples correlates with a better clinical outcome. Biochemically, we find that RasGRP1 creates a negative feedback loop that limits proliferative EGFR–SOS1–Ras signals in CRC cells. Genetic *Rasgrp1* depletion from mice with either an activating mutation in *KRas* or with aberrant Wnt signalling due to a mutation in *Apc* resulted in both cases in exacerbated Ras–ERK signalling and cell proliferation. The unexpected opposing cell biological effects of EGFR–RasGRP1 and EGFR–SOS1 signals in the same cell shed light on the intricacy of EGFR-Ras signalling in normal epithelium and carcinoma.

Thirty per cent of metastatic cancers carry somatic *KRAS* mutations (termed *KRAS^MUT* here), such as *KRAS^G12D*, which impair RasGAP-mediated Ras inactivation, culminating in high levels of active KRAS-GTP and strong proliferative signals[1–3]. Colorectal cancer (CRC) is the third most common cancer in the United States[4] and tumours carry *KRAS^MUT* in approximately 40% of patients[5]. Epidermal growth factor receptor (EGFR) expression is widespread in CRC (ref. 5) but clinical trials with anti-EGFR blocking antibodies or EGFR kinase inhibitors have been disappointing for CRC, particularly when tumours carry *KRAS^MUT* (refs 6,7). In contrast, such therapies have been successful in non-small-cell lung cancer patients with EGFR mutations[7]. The most intuitive explanation for failure of anti-EGFR therapy is that constitutive activity of *KRAS^MUT* bypasses regulation mediated by EGFR. However, EGFR signalling is essential for *KRAS^MUT*-driven pancreatic ductal carcinoma (PDAC) in mice[8,9] and in the clinic erlotinib is beneficial for some PDAC patients[10]. EGFR-Ras signalling in intestinal progenitor cells is believed to balance proliferation and differentiation[11], although mechanistic insights are limited.

Ras is GTP-loaded by Ras guanine nucleotide exchange factors (RasGEFs) in response to receptor signals[3]. The amplitude and duration of EGFR signalling to Ras and its downstream target MAPK (MAP kinase) affects cell fate; EGF stimulation of rat adrenal pheochromocytoma (PC-12) cells leads to transient Ras activation and proliferation whereas NGF stimulation results in sustained Ras-MAPK activation, exit from mitosis, and differentiation[12]. Lymphocytes also exhibit distinct Ras-MAPK activation patterns[13,14] and deficiency of Rasgrp1 or Sos1 RasGEFs impact T-cell development at distinct stages[15–18]. We have shown that the type of RasGEF dictates Ras activation patterns; RasGRP1 (Ras guanine nucleotide releasing protein-1) transmits analogue Ras signals whereas SOS1 (Son of Sevenless-1) transmits digital Ras signals[14]. Digital Ras activation relies on allosteric activation of SOS, accomplished by Ras-GTP binding to an allosteric pocket in SOS (ref. 19), creating a positive feedback loop in cells[14,20,21].

We established that RasGRP1 is structurally distinct from SOS1 and lacks allosteric activation by Ras-GTP (refs 19,22) and postulated that these RasGEFs may play distinct roles in EGFR signalling in the intestine. Here we reveal that RasGRP1 opposes EGFR-SOS1 signals and suppresses proliferation in normal intestinal epithelial cells as well as in epithelium carrying *KRas^G12D* or *Apc^Min/+* mutations. Our results reveal significant insights into the EGFR–Ras pathway and how nuances in EGFR-Ras signals impact cell biology.

## RESULTS

### RasGRP1 expression in CRC

We used a DT40 B-cell model engineered to express EGFR (ref. 23) to explore the effects of RasGEF deficiency on EGFR-induced ERK activation. We found that ERK activation is not only reduced in EGF-stimulated DT40 cells that lack SOS RasGEFs but also in cells lacking RasGRPs (Fig. 1a,b). SOS1 is ubiquitously expressed but RasGRP1 has specific expression patterns in cells of the immune system, skin and brain[15]. *Rasgrp1*-deficient mice have a T-cell development defect[17], suggesting an immune cell-centric role for Rasgrp1. However, Rasgrp1 was identified in fibroblast transformation assays[24], arguing that Rasgrp1 affects

the function of multiple cell lineages. Our DT40 data implied that RasGRP1 might play an unappreciated role in EGFR signalling and epithelial cell lineages.

We next used cBioPortal[25] to mine The Cancer Genome Atlas (TCGA) for RasGRP1 and plotted *RasGRP1* expression levels in 60 cancer cell lines (NCI-60 panel[26]). High expression of this RasGEF occurs in T-cell leukaemia lines MOLT4 and CEM, as we previously reported[27], but low-level *RasGRP1* expression exists in various CRC cell lines (Fig. 1c). *RasGRP1* messenger RNA levels covered a dynamic range in 56 established CRC cell lines (Fig. 1d) and in 276 CRC patient samples (Fig. 1e). The *RasGRP1* expressed typically consists of the wild-type (WT) sequence, and variants in *RasGRP1* are rare in CRC samples (5 out of 276, Fig. 1e). Similar ranges of *RasGRP1* expression levels are observed for $KRAS^{WT}$ or $KRAS^{MUT}$ CRC (Fig. 1f), an observation we confirmed in liver metastases of CRC patients (Fig. 1g). We next used the Oncomine database (www.oncomine.org) and uncovered that the *RasGRP1* expression levels in colonic adenocarcinomas are lower when compared with normal colonic epithelium (Fig. 1h), suggesting that RasGRP1 may play a protective role in CRC.

## Rasgrp1 regulates homeostasis of normal intestinal epithelial cells

Wnt signals at the bottom of intestinal crypts regulate self-renewal of stem cells and produced daughter cells undergo proliferation in response to EGFR signals, followed by terminal differentiation, migration and apoptosis[28]. In *Drosophila*, EGFR signalling is critical for intestinal maintenance[29,30]. In the mouse, deficiency in *Egfr* results in disorganized crypts[31] and fine-tuning of EGFR signalling is critical to regulate proliferation in the intestinal stem cell niche[32]. In the human intestine, EGFR-Ras signalling occurs in progenitor cells in the transit-amplifying (T/A) zone in the intestinal crypts, where it is thought to control proliferation and differentiation[11].

Immunohistochemistry revealed Rasgrp1-positive cells in crypts (Fig. 2a). *Rasgrp1*^{−/−} mice do not exhibit gross intestinal abnormalities but alterations may be revealed under circumstances of injury. We exposed *Rasgrp1*^{−/−} mice to a well-established model of colitis[33]. Remarkably, *Rasgrp1*^{−/−} mice showed partial protection from DSS (dextran sulphate sodium)-induced colitis (Fig. 2b,c). The lack of T lymphocytes in *Rasgrp1*^{−/−} mice is unlikely to provide protection because DSS induces colitis in models devoid of T lymphocytes[33]. We postulated that protection could stem from an intrinsic difference in *Rasgrp1*^{−/−} epithelial cells. *In vivo* BrdU labelling at 2 h (Fig. 2d) and 48 h (Fig. 2e) revealed that colonic intestinal epithelial cells without *Rasgrp1* proliferate more extensively compared with wild-type cells (Fig. 2f). In the *Rasgrp1*-deficient small intestine, BrdU^{+} cells were found at the top of the villus, 2 days after BrdU administration, whereas the furthest-progressed WT BrdU^{+} cells positioned midway along the crypt–villus axis (Fig. 2g,h). We also observed increased numbers of cleaved caspase-3-positive cells in *Rasgrp1*^{−/−} mice compared with WT mice (Fig. 2i,j). Thus, Rasgrp1 deficiency alters normal intestinal homeostasis and leads to increased proliferation accompanied by increased apoptosis at the tip of the villi. Loss of Rasgrp1 resulted in small but consistent increases in mucus-producing goblet cells (Fig. 2k,l), which may provide an additional explanation for the reduced DSS colitis in *Rasgrp1*^{−/−} mice.

## Deletion of Rasgrp1 exacerbates intestinal dysplasia in *KRas$^{G12D}$* mice

We next explored the role of RasGRP1 in the context of *KRAS$^{MUT}$*, a somatic mutation found in ~40% of CRC patients[5]. Expression of *KRas$^{G12D}$* in the intestinal epithelium of mice produces aberrant cell proliferation and hyperplasia accompanied by relatively intact terminal differentiation[34–36]. We reduced the Rasgrp1 expression in *VillinCre:KRas$^{LSL-G12D}$* mice[35] (termed *KRas$^{G12D}$* here) by crossing them to *Rasgrp1$^{-/-}$* mice[17]. We used *VillinCre* mice as control (termed wild type—WT—here). Heterozygosity for *Rasgrp1* results in half the Rasgrp1 protein dosage[37], whereas *Rasgrp1*-deficient mice express no Rasgrp1 protein[17] (Fig. 2a).

In the normal colon, proliferation is confined to cells in the bottom of the crypt. *KRas$^{G12D}$* mice exhibited colonic crypt hyperplasia with increased numbers of proliferating cells further up in the differentiated zone, measured through Ki67 staining or *in vivo* BrdU labelling. Loss of Rasgrp1 resulted in a further augmentation of the *KRas$^{G12D}$*-induced proliferation (Fig. 3a–c and Supplementary Fig. 1a,b). Serrated dysplasia is a notable feature of the *KRas$^{G12D}$* mouse colon and seen in *KRAS$^{MUT}$* human hyperplastic polyps[34–36] (Fig. 3a,b). At 6 months of age, we found that loss of either one or both *Rasgrp1* alleles resulted in exacerbated serrated dysplasia, typified by further lengthening and increased serration of villi-like projections into the colonic lumen, and accompanied by increased abundance of goblet cells (Fig. 3d,e and Supplementary Fig. 1c). The increased goblet cell presence and heavily serrated nature in these *KRas$^{G12D}$:Rasgrp1$^{WT/-}$* and *KRas$^{G12D}$:Rasgrp1$^{-/-}$* mice share remarkable resemblance with human hyperplastic or serrated polyps of the goblet cell subtype[38], an important subcategory of hyperplastic polyps that provides a route to CRC distinct from conventional adenomas to CRC (ref. 38).

In the normal small intestine, proliferation mainly takes place in the crypt and T/A zone, which is one epithelial cell layer thick[28] and the site of EGFR signalling[11]. Compared with WT controls, villi of *KRas$^{G12D}$* small intestine were longer and had a branched appearance in 20% of the cases, as suggested previously[36]. Depletion of *Rasgrp1* in the context of *KRas$^{G12D}$* resulted in a more profound branching of the villi (Fig. 3f–i and Supplementary Fig. 2a,b). Second, expression of *KRas$^{G12D}$* resulted in thickening and increased cellularity of the T/A zone, accompanied by an expansion of Ki67-positive cells higher up on the crypt–villus axis (Fig. 3j,k,n,o). Deletion of *Rasgrp1* exacerbated this feature of the *KRas$^{G12D}$* phenotype substantially; we observed 15- to 20-cell-wide T/A zones of pseudo-stratified cells positive for Ki67 and with heterochromatin features (Fig. 3l,m,p,q). These characteristics are indicative of active cell division and used to type dysplastic tissues from patients[38]. Despite increases in proliferation, deletion of *Rasgrp1* did not trigger further lengthening of already elongated *KRas$^{G12D}$* villi nor did it lead to an overall increase in length of the intestinal track (Supplementary Fig. 2c,d). Instead, we observed increased levels of cleaved caspase-3 when Rasgrp1 is deleted in the context of *KRas$^{G12D}$* (Fig. 3r,s). As previously reported[36], we did not see differences in apoptosis between *KRas$^{G12D}$* and WT small intestines.

## EGFR-RasGRP1 and EGFR-SOS1 signals in epithelial cells

Our genetic approach reveals that Rasgrp1 restricts the dysplastic effects of $KRas^{G12D}$ in the intestinal epithelium. To investigate the underlying mechanism, we first established RasGRP1 protein expression in 16 of 18 human CRC cell lines as well as EGFR expression (Fig. 4a). Eleven of eighteen CRC cell lines carried the stereotypic $KRAS^{MUT}$ found in patients[5].

In stimulated lymphocytes, the GEF activity of RasGRP1 is enhanced through PKC-dependent phosphorylation[15]. We used the DT40 cell system to demonstrate that phospho-$T_{184}$-RasGRP1 levels were induced on B-cell receptor-but also EGFR-stimulation in RasGRP- and PKC-dependent manners (Fig. 4b). We subsequently immunoprecipitated RasGRP1 from $KRAS^{WT}$ SW48 and $KRAS^{MUT}$ HCT15 CRC cells, two lines of similar stage (Dukes' type C colorectal adenocarcinoma, ATCC information). EGF transiently elevated phosphorylation of RasGRP1 in both lines (Fig. 4c). SOS1, pre-complexed with Grb2, is recruited to phosphorylated Tyr 1068 in EGFR (ref. 39) and subject to feedback that includes EGF-induced phosphorylation[40]. Consequently, EGFR stimulation induced a mobility shift of SOS1 in HCT15 and SW48 cells (Fig. 4d). To investigate the RAF–MEK–ERK effectors pathway downstream of RasGTP, we examined ERK phosphorylation and noted that both cell lines exhibit EGF-induced activation of ERK kinases (Fig. 4e). RasGRP1 and SOS1 probably play roles in CRC cells with either a $KRAS^{MUT}$ or a $KRAS^{WT}$ allele, because both RasGEFs are phosphorylated in HCT15 and SW48 cells in response to EGF (Fig. 4f).

## $KRAS^{MUT}$ CRC cell lines demonstrate EGFR-induced hyperactivation of RAS

To investigate the mechanistic underpinnings of RasGRP1, SOS1 and $KRAS^{MUT}$ in the cellular response to signalling through EGFR, we selected seven CRC lines that represent each significant genotype (Supplementary Table 1). Expression of $RasGRP1$ in these cells is specific and selective; these cell lines express essentially no $RasGRP3$ or $RasGRP4$. RasGRP2, although expressed, for example, in $CaCO_2$ and SW48 (Supplementary Fig. 3), is an exchange factor for the small GTPase Rap[15,41].

As expected from the impaired RasGAP-mediated inactivation of $KRAS^{MUT}$ (refs 1–3), lines carrying $KRAS^{MUT}$ exhibited elevated constitutive RAS-GTP levels compared with $CaCO_2$, WiDr and SW48 cells with $KRAS^{WT}$ (Fig. 5a). Low baseline KRAS-GTP levels were efficiently, but transiently, elevated by EGF stimulation of $KRAS^{WT}$ cell lines (Fig. 5b,d). Significantly, elevated constitutive KRAS-GTP levels in $KRAS^{MUT}$ CRC cells were further increased by EGF stimulation (Fig. 5c,d). This last observation, combined with our data in Fig. 4, suggests that EGFR acts through RasGEFs to provide further exchange factor input to hyperactivate KRAS in $KRAS^{MUT}$ cells. Moreover, N-and HRAS demonstrated the same pattern of sustained activation in $KRAS^{MUT}$ cells and transient activation in $KRAS^{WT}$ cells (Fig. 5e–h).

Allosteric activation of SOS by Ras-GTP greatly enhances its RasGEF activity[19] and creates a positive feedback loop in cells[14,20,21] (Fig. 5i). Recent work revealed that $KRAS^{MUT}$ primes SOS in unstimulated PDAC cell lines and results in elevated constitutive levels of

HRAS-GTP (ref. 42). Our RAS-GTP pulldown experiments demonstrate that allosteric SOS1 activation by $KRAS^{MUT}$ may also play a role in cancer cells under the condition of EGF stimulation (Fig. 5i).

### SOS1 promotes EGF-induced KRAS activation and growth of $KRAS^{MUT}$ CRC cells

To explore how SOS1 and RasGRP1 shape the character of EGFR-Ras signals and impact cell biology in the context of $KRAS^{MUT}$, we first reduced human SOS1 expression in HCT15 CRC cells, which respond to EGF but are insensitive to EGFR inhibitor erlotinib (Fig. 6a and Supplementary Table 2). Reduction of SOS1 expression resulted in: less sustained KRAS activation following EGF stimulation, compared with controls (Fig. 6b); diminished *in vitro* colony formation, particularly noticeable when dependent on EGF (Fig. 6c,d); and reduced *in vivo* tumorigenesis when subcutaneously xenografted (Fig. 6e). These results demonstrate that EGFR-SOS1-Ras signals contribute to tumorigenesis when CRC cells carry a $KRAS^{MUT}$ allele.

### RasGRP1 restricts EGF–SOS1-induced KRAS-ERK signalling through negative feedback

We postulated that reduction of RasGRP1 expression in HCT15 cells (Fig. 7a) may have a different outcome, because RasGRP1 is structurally distinct from SOS1, is not activated allosterically by RAS-GTP, and possesses 1,000-fold lower intrinsic RasGEF activity[22]. A 53% reduction of RasGRP1 from HCT15 cells resulted in increased EGFR-driven hyperactivation of KRAS (Fig. 7b), which translated into sustained ERK phosphorylation downstream of Ras-GTP (Fig. 7c,d and Supplementary Fig. 4a,b).

We subsequently investigated whether RasGRP1 may impact SOS1. We examined levels of P-Y$_{1068}$-EGFR (phospho-tyrosine 1068 in EGFR) a major auto-phosphorylation site[43] to which Grb2-SOS1 is recruited[39], under conditions of EGF stimulation (Fig. 5i). Reduction of RasGRP1 expression significantly and selectively increased P-Y$_{1068}$-EGFR levels (Fig. 7e) and increased levels of P-Y$_{1068}$-EGFR complexed to SOS1-Grb2 (Fig. 7f). RasGRP1 is recruited to the membrane by diacylglycerol[15] and enhancing diacylglycerol–RasGRP1 signalling in EGF-stimulated HCT15 cells through exposure to an inhibitor of the diacylglycerol-converting enzyme DGK (diacylglycerol kinase)[44] resulted in reduced P-Y$_{1068}$-EGFR levels (Fig. 7g). Thus, diacylglycerol–RasGRP1 signalling constitutes a negative feedback loop to limit P-Y$_{1068}$-EGFR-Grb2-SOS-RAS-ERK signals.

Analogous to our findings in the human CRC HCT15 cell line, we observed that deletion of one or two alleles of *Rasgrp1* in the context of $KRas^{G12D}$ substantially increased the relative staining for phosphorylated ERK kinases in sections of colonic epithelium (Fig. 7h). Furthermore, direct, side-by-side comparisons of isolated epithelial cells confirmed the increased ERK phosphorylation in $KRas^{G12D}$ colonic epithelial cells when Rasgrp1 levels are reduced (Fig. 7i).

### RasGRP1 expression levels limit growth of $KRAS^{MUT}$ CRC cells

Reduction of RasGRP1 expression led to increased colony formation of HCT15 CRC cells *in vitro*, induced by either serum or by EGF (Fig. 8a,b), and increased size and enhanced growth rate of xenografted tumours, compared with the parental HCT15 cells or HCT15

cells with a mouse Rasgrp1 short hairpin RNA (shRNA) construct as specificity controls (Fig. 8c,d). Thus, diacylglycerol–RasGRP1 signalling constitutes a negative feedback loop that limits EGFR-SOS-RAS signalling and has a growth-suppressive role.

To investigate whether levels of RasGRP1 in CRC impact patients clinically, we explored three published gene expression studies linked to clinical outcome of CRC patients (GSE17536 (ref. 45); GSE12945 (ref. 46); GSE14333 (ref. 47)). We applied an established cutoff finder[48] to divide CRC patients into two groups based on RasGRP1 expression. We observed that high expression of RasGRP1 correlates with a better clinical outcome (Fig. 8e and Supplementary Fig. 5a,b).

### RasGRP1 suppresses proliferative ERK signalling in the context of aberrant Wnt signalling

CRC from patients in the above-mentioned studies do not all contain $KRAS^{MUT}$ and low RasGRP1 levels may therefore also lead to worse clinical outcome of CRC caused by other (non-$KRAS^{MUT}$) genetic lesions. To test this possibility, we next explored the $Apc^{Min/+}$ mouse model ($APC$: adenomatous polyposis coli) with aberrant Wnt signalling[49] that is widely used to model human CRC (refs 50–52). Crosses of $Apc^{Min/+}$ mice to $Rasgrp1$-deficient mice revealed that mean survival of 164 days for $Apc^{Min/+}$ mice diminished to 126 days when $Apc^{Min/+}$ mice were also deficient for $Rasgrp1$ (Fig. 8f). As reported[50–52], we found large numbers of tumours in the $Apc^{Min/+}$ small intestine. Additional loss of $Rasgrp1$ did not lead to significant changes in tumour numbers or size in the small intestine (Fig. 8g,h) but led to a significant increase in the number of colonic tumours, which rarely develop in $Apc^{Min/+}$ mice (Fig. 8i,j). Colonic tumours in $Apc^{Min/+}:Rasgrp1^{-/-}$ or $Apc^{Min/+}$ mice demonstrated a similar overall architecture (Fig. 8k and Supplementary Fig. 6a) but exhibited increased individual tumour size (Fig. 8l). In agreement, normal crypts and tumours of $Apc^{Min/+}:Rasgrp1^{-/-}$ mice revealed increases in proliferative markers compared with Apc$^{Min/+}$ mice (Fig. 8m,n and Supplementary Fig. 6b). Moreover, loss of Rasgrp1 resulted in significant increases in phospho-ERK signals in both the normal crypts and in tumours in the context of $Apc^{Min/+}$ (Fig. 8o). Cleaved caspase-3-positive, apoptotic cells were rare in $Apc^{Min/+}$ tumours and remained sparse, although slightly increased, in tumours from $Apc^{Min/+}:Rasgrp1^{-/-}$ mice (Fig. 8p and Supplementary Fig. 6c). Thus, RasGRP1 plays a suppressive role in CRC in the context of both $KRAS^{MUT}$ and $Apc^{Min/+}$ by limiting proliferative ERK signals.

## DISCUSSION

Here we revealed that RasGRP1 and SOS1, two structurally distinct RasGEFs (refs 19,22), both lie downstream of EGFR. Reduction of RasGRP1 levels relieves the negative feedback to EGFR-SOS1, sustains EGFR-RAS-ERK signalling, and promotes cell proliferation. We find that RasGRP1 plays a negative regulatory role in CRC and that depletion of $Rasgrp1$ alleles exacerbates ERK signalling and serrated dysplasia and hyperproliferation of the $KRas^{G12D}$ intestinal epithelium. $KRas^{G12D}$ alone does not lead to full CRC in mice[34–36]. Consistent with the conclusion that perturbed Ras function by itself is insufficient to produce CRC, we did not observe high-grade dysplasia or adenocarcinomas in $KRas^{G12D}:Rasgrp1^{WT/-}$ and $KRas^{G12D}:Rasgrp1^{-/-}$ mice that were up to 9 months of age.

Epithelial cells in these two models return to the normal simple columnar pattern further up the villus, despite the severely altered T/A zone, and loss of *Rasgrp1* results in increased levels of cell apoptosis. For full CRC to develop in mice, *KRas*[G12D] requires additional events such as loss of the *APC* tumour suppressor[35]. Vice versa, perturbation of APC requires EGFR signalling for tumour maintenance[53,54]. In agreement with the concept that these two pathways intersect in CRC, we observe that loss of *Rasgrp1* in addition to the *Apc*[Min/+] allele leads to increases in colonic tumour numbers and sizes and reduced mean survival of *Apc*[Min/+]:*Rasgrp1*^{−/−} mice.

RasGRP3 seems to connect to cMET(HGF)- signal input[55]. Our results here show that RasGRP1 responds to EGFR signal input. Thus, RasGRP RasGEFs can couple to receptor tyrosine kinases but the mechanistic details and the biological consequences are not yet fully understood. RasGRP3 promotes growth of melanoma- and prostate-cancer cells[55,56] whereas our findings here demonstrate that RasGRP1 opposes CRC growth. The suppressive function of RasGRP1 in CRC also contrasts its growth-promoting role in T-cell leukaemia[27] and in skin cancer[57]. Thus, not all RasGRP1-generated Ras signals are the same and RasGRP1 may function as a context-dependent tumour-suppressor protein or a protein with oncogenic functions.

Here we revealed non-intuitive feedback between two RasGEFs; that is, EGFR-RasGRP1 signals that dampen EGFR-SOS signals. Grb2 can impair access of phosphatases to the FGFR (refs 58,59). Possibly, RasGRP1 indirectly promotes phosphatase access to EGFR, reducing Grb2-SOS1-P-Y$_{1068}$-EGFR complexes. Alternatively, EGFR-RasGRP1 may influence phosphatase function directly. The phosphatase Cdc25A binds to and dephosphorylates EGFR (ref. 60). Interestingly, vemurafenib (PLX4032) treatment of CRC cells with somatic *BRAF(V600E)* was recently shown to relieve a negative feedback loop to EGFR by decreasing the activity of the phosphatase Cdc25C, resulting in increased P-Y$_{1068}$-EGFR levels[61]. It is of interest to note that somatic *KRAS*[MUT] emerge as mediators of acquired resistance to anti-EGFR therapy[62,63]. Possibly anti-EGFR therapy inhibits the negative feedback coming from EGFR-RasGRP1 signals.

## METHODS

### Bioinformatics and TCGA data mining

NCI-60 cell lines[26], Cancer Cell Line Encyclopedia[64] and Colorectal Adenocarcinoma[65] databases were evaluated for *RasGRP1* mRNA expression and copy levels. We used the bioinformatics tool 'cBio Cancer Genomics Portal'[25] to interrogate the above cancer genomic databases (www.cbioportal.org). We analysed *RasGRP1* mRNA expression *z*-scores correlated with copy number level in NCI-60 cell lines, Cancer Cell Line Encyclopedia and The Cancer Genome Atlas (TCGA) Colorectal Adenocarcinoma, and we computed the *KRAS* mutation association *z*-score with *RasGRP1* mRNA expression[25].

We compared *RasGRP1* gene expression in human colon cancer and normal tissues using the Oncomine database (www.oncomine.org). Statistical analysis of the differences in *RasGRP1* expression between these tissues used Oncomine standard algorithms: for each microarray, data were log$_2$-transformed, median-centred, and standard deviation

normalized[67]. The TCGA data set obtained from Oncomine is embedded in the TCGA database (https://tcga-data.nci.nih.gov/tcga).

To validate the correlation for *RasGRP1* expression and patient outcome, three public colon cancer data sets (GSE17536 (ref. 45); GSE12945 (ref. 46); GSE14333 (ref. 47)) were downloaded from the NCBI GEO database (National Center for Biotechnology Information, Gene Expression Omnibus). Data were normalized using the Robust Multichip Average (RMA) and annotated in GEO (ref. 68). A cutoff finder using the R statistical engine was performed to define two groups of patients with different survival curves using RasGRP1 gene expression (low or high)[48]. We analysed data at a follow-up time of ten years. The Kaplan–Meier estimator was used to evaluate patients' prognosis. The log-rank (Mantel–Cox) test was carried out to compare survival curves and to measure hazard ratios. Analyses were performed and graphs were generated using GraphPad Prism version 6.04.

### Cell lines and reagents

Cell lines were cultured at 37 °C in 5% $CO_2$. Stable cell lines infected with lentivirus containing small hairpin RNA (shRNA) against SOS1 or RasGRP1 were selected with puromycin 10 μg ml$^{-1}$ (Mediatech, Cellgro) and subsequently sorted for GFP levels. Cells were maintained under selection. Colorectal cancer (CRC) cell line mutational status was obtained from the Wellcome Trust Sanger Institute Cancer Genome Project website (http://www.sanger.ac.uk/genetics/CGP) and verified by UCSF sequencing core facility (Supplementary Table 1). BrdU, DAPI and Alcian blue were purchased from Sigma-Aldrich, diacylglycerol kinase inhibitor II (R59949) was purchased from Enzo Life Science (Alexis) and dissolved in DMSO, human epithelial growth factor (hEGF) recombinant protein was purchased from Life Technologies and dissolved in PBS, and PKC inhibitor rottlerin was purchased from Calbiochem and dissolved in DMSO.

### Antibodies

Antibodies were obtained from the following sources and used at the indicated concentration: SOS1 (1:1,000 for western blot; 1:100 for immunoprecipitation) from BD Bioscience (610095, clone 25/SOS1); α-tubulin (1:2,000; T6074) from Sigma-Aldrich; anti-Ras (1:1,000) from Millipore (03-516, clone RAS10); Grb2 (sc-255, C-23), KRas (sc-30, F234), NRas (sc-31, F155) and HRas (sc-520, C-20) (1:200) from Santa Cruz Biotechnology; epithelium growth factor receptor (EGFR; no. 2646), phospho-EGFR (Y-1068; no. 3777, D7A5), phospho-EGFR (Y-1045; no. 2237), phospho-ERK1/2 (no. 4370), ERK1/2 (no. 9102; 1:1,000) and cleaved caspase-3 (Asp 175; no. 9661; 1:200) from Cell Signaling Technology; Ki-67 (1:500; ab15580) from Abcam; anti-BrdU from the Developmental Study Hybridoma Bank (G3G4, 1:300), murine RasGRP1 (m199; immunoprecipitation 1:50) from J. Stone (University of Alberta, Edmonton, AB, Canada); human RasGRP1 (JR-E160; 1:1,000) generated by our laboratory together with Epitomic, phospho-RasGRP1-T184 was generated by immunization with the peptide SRKL-pT-QRIKSNTC by our laboratory and Eurogentec/AnaSpec.

## Mice and patient samples

Mice were handled according to the Institutional Animal Care and Use Committee regulations, described in the Roose laboratory University of California, San Francisco (UCSF) mouse protocol AN084051 'Ras Signal Transduction in Lymphocytes and Cancer'. $KRas^{LSL-G12D/+}$ mice ($KRas^{G12D}$, here) previously described were kindly provided by T. Jacks (MIT). We crossed these mice to VillinCre transgenic mice to activate the mutant *KRAS* allele in the intestinal tract. This mouse was used as a control and noted WT. Progenies were then crossed to a Rasgrp1 knockout ($Rasgrp1^{-/-}$) provided by J. Stone to generate a mouse expressing $KRas^{G12D}$ *in the context of 1 and 2 Rasgrp1 alleles deleted* $KRas^{G12D}$:*Rasgrp1$^{WT/-}$* and $KRas^{G12D}$:*Rasgrp1$^{-/-}$* respectively. $Apc^{Min/+}$ mice were crossed to $Rasgrp1^{-/-}$ mice to obtain complete deletion of Rasgrp1($Apc^{Min/+}$:*Rasgrp1$^{-/-}$*). Primers used for genotyping of Rasgrp1: Primer 1, 5′-GCAGCTGTCAATAAGATCATCCAGGC-3′; primer 2, 5′-ATATTGCTGAAGAGCTTGGCGGCGAATGGG-3′; primer 3, 5′-CTATCCTCACTTGAGTCTCTCTTTCC-3′. All other primers were recommended by Jackson laboratory.

The utilization of resected or biopsied liver metastases from primary CRC for the purpose of evaluation of potential biomarkers of clinical outcome was approved by the University of California San Francisco committee on Human Research and patient consent was obtained. Decoded CRC patient samples obtained from R.W. were analysed by the Roose group for RasGRP1 expression (CHR approval - Study Title: RasGRP1 in Human T cell lymphoma and CRC IRB no.: 12-09467; reference no.: 053353).

## shRNA constructs and experiments

Knockdown of human RasGRP1 and human SOS1 has been described previously[11]. The oligonucleotide sequences are as follows. For mRasgrp1-1503: sense oligonucleotide, 5′-TGATCGCTGCAAGC-TTTCCATTCAAGAGATGGAAAGCTTGCAGCGATCTTTTTTC-3′; antisense oligonucleotide, 5′-TCGAGAAAAAAGATCGCTGCAAGCTT-TCCATCTCTTGAATGGAAAGCTTGCAGCGATCA-3′. For hRasGRP1-1503: sense oligonucleotide, 5′-TGATT--GCTGCG--AGT--TTTCCATTCA-AGAGATGGAAAACTCGCAGCAATCTTTTTTC-3′; antisense oligonucleotide, 5′-TCGAGAAAAAAGATTGCTGCGAGTTTTCCATCTC-TTGAATGGAAAACTCGCAGCAATCA-3′. Targeting of the 1503 region was based on previous work[21]. The hRasGRP1-1503 targets human RasGRP1, has three mismatches with the same sequence in mRasgrp1-1503, and served as a specificity control. CRC cell lines were seeded in 24-well plates and infected with lentivirus (5MOI) with Polybrene through standard spin infections (1,044*g* for 1 h) and selected on puromycin (10 μg ml$^{-1}$) 48 h after infection. Similarly, SOS was targeted as described previously[11]. hSOS1-1313 targets human SOS1, has two mismatches with the same sequence in mSos1-1313, and served as a specificity control. For mSos1-1313: sense oligonucleotide, 5′-TGACAGTGTTGCAA-TGAGTTTTCAAGAGAAACTCATTGCAACACTGTCTTTTTTC-3′; antisense oligonucleotide, 5′-TCGAGAAAAAAGACAGTGTTGCAAT-GAGTTTCTCTTGAAAACTCATTGCAACACTGTCA-3′. For hSOS1-1313: sense

oligonucleotide, 5′-TGACAGTGTTGT--AATGAA--TTTTCAAGA-GAAATTCATTACAACACTGTCTTTTTTC-3′; antisense oligonucleotide, 5′-TCGAGAAAAAAGACAGTGTTGTAATGAATTTCTCTTGA-AAAATTCATTACAACACTGTCA-3′.

### RNA extraction and real-time PCR

Total RNA was isolated from human tissue and cell lines using RNeasy kit (Qiagen). RNA was reverse-transcribed with random primers (Invitrogen) and Moloney murine leukaemia virus reverse transcriptase. Real-time PCR was performed in triplicate using Eppendorf RealPlex2. Gene expression was normalized to that of GAPDH and quantified with the comparative CT method according to the manufacturer's instructions. The following combinations of primers and probes were used to analyse the expression of human RasGRP1: forward, 5′-AAGCTCCACCAACTACAGAACT-3′; reverse, 5′-AGGGAGATGAGGTCCTTGAGAT-3′; probe, FAM-5′-CCACATGAAATCAATAAGGTTCTCGGTGAG-3′-TAMRA and human GAPDH forward, 5′-GAAGGTGAAGGTCGGAGT-3′; reverse, 5′-GAAGATGGTGATGGGATTTC-3′; probe, FAM-5′-AGGCTGAGAACGGGAAGCTTGT-3′-TAMRA. RasGRP2, 3 and 4 probes and primers were obtained at Applied Bio System. For patient samples the sample size ($n= 30$) was based on the number of samples with high-quality RNA.

### Western blot

Cells were plated in 6 or 10 cm dishes and starved for 2 h at 37 °C in PBS. After resting, cells were EGF-stimulated for different times: 3, 10 or 30 min. Cells were lysed with ice-cold 2% NP40 supplemented with protease and phosphatase inhibitors (10 mM sodium fluoride, 2 mM sodium orthovanadate, 0.5 mM EDTA, 2 mM phenylmethylsulphonyl fluoride, 1 mM sodium molybdate, aprotinin (10 mg ml$^{-1}$), leupeptin (10 mg ml$^{-1}$), pepstatin (1 mg ml$^{-1}$)). After 30 min on ice, lysates were centrifuged and the supernatants were mixed with 2× sample buffer. Protein lysates were separated on acrylamide gel 10%, transferred on PVDF membrane and incubated with the primary antibodies of interest. Inhibitors such as rottlerin (20 μM) and DGK were pre-incubated for 30 min before stimulation. Western blots were visualized with enhanced chemo-luminescence and imaging on a Fuji LAS 4000 image station (GE Healthcare). The protein bands in western blots were quantified with Multi Gauge software, and densitometry (pixel intensity) was determined within the linear range of the exposure. Amounts of the proteins of interest were typically presented as a ratio of the indicated loading control. Values were then normalized to an indicated sample and noted as a fold difference.

### Ras pulldown assay

Activation of Ras was analysed by a Ras-GTP pulldown assay. Cells were rested in PBS with Ca/Mg in 6-well plates at 37 °C for 2 h and stimulated with 5 ng ml$^{-1}$ hEGF for 3 and 10 min. Cells were then lysed with ice-cold 1× MLB for pulldowns (Millipore) and scraped. Twenty per cent of the lysate was used for whole-cell lysate and 80% was used for pulldown according to the manufacturer's instructions (Upstate). Lysates were loaded on precast bis-

tris gel 4–12% (Invitrogen). Membranes were incubated with primary antibody and specific signals have been quantified as described in the western blot paragraph.

## Immunoprecipitation

Cells were grown in 10 cm dishes and starved for 2 h at 37 °C in PBS. After resting, cells were EGF (5 ng ml$^{-1}$ or 25 ng ml$^{-1}$) stimulated for 3, 10 or 30 min and lysed in 1% NP40 as described above. The supernatant was split into 2 parts. 20% was used for whole-cell lysates and 80% was incubated with anti-human SOS1 and tumbled for 2 h at 4 °C. The G-Sepharose beads (GE Healthcare) were added and tumbled for 50 min at 4 °C. After several washes using 1% NP40, sample buffer was added before being boiled and loaded on acrylamide gels 8% and 10%. Results represent at least three independent experiments.

## Isolation of intestinal epithelial cells

Methods were adapted from ref. 69. In short, large intestines were dissected, rinsed with PBS, opened and cut into 1–2 cm fragments before incubation in a conical tube with PBS. Debris was removed by PBS washes and fragments were transferred to clean tubes containing pre-warmed PBS with 2.5 mM EDTA. Fifteen-min incubations at 37 °C in a water bath and removal of supernatant containing epithelial cells at crypt structures were repeated 2–3 times and cells were collected by centrifugation at 311$g$ and cells were lysed in NP40 lysis buffer to extract proteins.

## Extraction of colonic epithelium and tumours

Colon of mice were dissected and washed with PBS. Tumours were isolated and flash-frozen. Healthy tissues adjacent to tumours were collected to serve as controls. Tissues were incubated in 200 μl of 1× RIPA buffer on ice and homogenized using an electric dounce. Lysates were process as described elsewhere. Protein quantification was evaluated using BCA assay (Thermo Scientific).

## Soft-agar colony formation assay

Colorectal cell lines were seeded (1 × 10$^5$) in duplicate into 60-mm cell culture dishes in 1 ml of 0.3% agar (Noble agar, SIGMA) in RPMI containing 5% FBS, 1% penicillin/streptomycin, 1% glutamine, and 2.37 g l$^{-1}$ Na$_2$CO$_3$, on top of a layer of 1 ml of 1% agar. For complete culture conditions, normal culture media was added and changed every other day. Cultures were maintained for 15 days. For the EGF condition, hEGF (10 ng ml$^{-1}$) was added to minimal culture media. Colonies were fixed with 70% ethanol and stained with 0.005% crystal violet. Colonies were visualized, and at least 5 randomly chosen fields were photographed with a Nikon DXM1200 digital camera coupled to a light microscope. Results are a combination of three-independent experiments.

## Xenograft mouse studies

HCT15 cells with or without shRNA (2 × 10$^5$) were injected subcutaneously into the flank of 6- to 8-week-old male Nude-Foxn1nu mice ($n$ = 5 at least per group; Harlan lab). Tumour volume was determined by external calliper measurement every other day as soon as it reached a palpable size. Calculation was carried out as follows: tumour volume=

$1/2(\text{length} \times \text{width}^2)$. Mice were monitored daily for body weight and general condition. According to institutional guidelines, mice were euthanized when their tumour volume reached 2,000 mm$^3$ or became excessively ulcerated. Experiments were repeated twice with 5 mice in each group, experiments were not randomized. Pilot studies guided our choice of sample size and gave an indication of the difference to be expected between experimental samples in the eventual experiments.

### Dextran sodium sulphate-induced colitis

DSS (3%, MP Biomedicals) was added to the drinking water of co-housed, 10–12-week-old C57Bl6 and Rasgrp1$^{-/-}$ mice for 5 days. Mice were assessed daily for diarrhoea, bloody stools and body weight. At day 5, mice were euthanized and the small and large intestines were processed as described in the immunohistochemistry section. DSS damage scores were determined by the sum of three parameters as previously described[66]: surface epithelial loss, crypt destruction, and inflammatory cell infiltration into the mucosa. A score of '0' represents no change, '1' localized and mild change, '2' localized and moderate change, '3' extensive and moderate change, '4' extensive and severe change.

### Immunohistochemistry

Tissues were dissected, fixed in 4% PFA and paraffin-embedded. Then 5-μm-thick sections were de-waxed in Histo-Clear (National Diagnostics) and rehydrated in graded alcohol baths. Antigen retrieval was performed in a pressure cooker for 20 min in 10 mM sodium citrate buffer, pH 6.0. For cleaved caspase-3 staining, a solution of 10 mM TRIS with 1 mM EDTA pH 9 was used. Endogenous peroxidase activity was inhibited with 1.5% H$_2$O$_2$ in methanol for 20 min and washed in PBS. Nonspecific binding sites were blocked in blocking buffer (PBS, pH 7.4, 3% serum, 1% BSA and 0.1% Tween) for 60 min at room temperature. Sections were then incubated with primary antibodies diluted in blocking buffer overnight at 4 °C. Slides were then washed twice with 0.1% PBS–Tween before incubation in Universal Immuno-peroxidase polymer anti-mouse/rabbit Histofine for mouse tissues (Nichirei Biosciences) was used as a secondary reagent. Stainings were visualized with DAB (3,3′-diaminobenzidine, Sigma-Aldrich) and a haematoxylin counterstain (Sigma-Aldrich) was performed before dehydration. After dehydration, sections were mounted in Cytoseal 60 (Thermo Scientific). To study the structure of tissue, haematoxylin & eosin (H&E) staining was performed. For quantification, images were acquired using a Nikon Optiphot microscope equipped with an AxioCam HR at fixed exposure (objective ×20 and ×40). For BrdU experiments, mice were injected intraperitoneally (2 mg per 200 μl) for 2 h or 48 h. To detect goblet cells, slides were treated with Alcian blue (pH 2.5) for 30 min and counterstained using Nuclear red (Sigma-Aldrich) followed by standard mounting techniques.

### Immunofluorescence

Tissues were dissected, fixed in 4% PFA, incubated overnight at 4 °C in sucrose 30% and embedded in OCT (Tissue-Tek)/sucrose 30% (2 vol/1 vol). Sections (10-μm-thick; Cryostat Leica) were dried and washed in PBS. After a 0.1% PBS–Tween (Sigma-Aldrich) wash, the sections were incubated in blocking buffer (1% BSA, 3% normal goat serum and 0.2% Triton X-100–PBS) for 1 h at room temperature. Sections were then incubated with primary

antibodies diluted in blocking buffer overnight at 4 °C and washed twice with 0.1% PBS–Tween and PBS before incubation in secondary antibody conjugated with Alexa 546 (Molecular Probes, Life technologies) and DAPI in PBS–Triton X-100 0.5% (Sigma-Aldrich) for 45 min at room temperature. Slides were washed twice with PBS before mounting with mounting medium (Dako). Images were taken by using a micro-lensed, spinning disk confocal scan-head coupled to a motorized, inverted fluorescence microscope (Zeiss Axiovert 200M; Carl Zeiss). Images were collected using an ICCD camera (XR-Mega-10EX S-30, Stanford Photonics).

### Positioning of *in vivo* BrdU-labelled cells

Mice were injected with BrdU as described before and euthanized 48 h post-injection. Swiss roll gut preparations were produced, stained and fixed as described above. BrdU-positive cells from 20 crypt–villus axes in duodenum were analysed per mouse. Cells were counted blind from the bottom (position 1) of open crypts (transversally sectioned) to the top of villi. The percentage of cells per position was representative of two mice per genotype. The counting method was adapted from ref. 49.

### Quantification and statistical analysis

In short-term BrdU experiments at 2 h after injection, 50 crypts were counted per mouse ($n$ = 3). For cleaved caspase-3 experiments (immunofluorescence), 120 open villi per genotype were counted ($n$= 3). For branching villi, a total of 120–150 villi per genotype ($n$ = 3 mice per genotype) were counted in different areas of the duodenum. For goblet cells in the intestine, 50 open villi (transversally sectioned) in the duodenum per mouse were counted; two mice per genotype. For goblet cells and Ki67-positive cells in colon, 50 crypts in the distal colon were counted with 3 mice per genotype. For cleaved caspase-3 and BrdU in tumours, numbers of positive cells were evaluated per field (100 μm × 100 μm) with 3 to 6 fields taken per tumour ($n$ = 3 mice per genotype). For villi lengths, pictures were taken and the length of the villi in the duodenum was determined using ImageJ software. Pixel values were transformed into metric values using a microscope scale. Fifty villi were counted and values are representative of three mice per genotype. All data were represented as mean ± s.e.m. For xenograft experiments, damage score after DSS treatment, and immunostainings, unpaired *t*-tests were used for two-group comparisons. For comparisons of phospho-ERK immunoblot quantification in $Apc^{Min/+}$ mice, a paired *t*-test was applied. All specific statistical analyses are mentioned in the respective paragraphs. Counting for Ki67 staining, brdU, goblet cells, cleaved caspase-3 and branching villi, was done blind. In all other experiments, a one-way ANOVA followed by a Bonferroni *post hoc* test was used for comparisons of three or more groups. For all tests, a *P* value of <0.05 was considered statistically significant. Analyses and graphs were done using Prism 5 software.

## Supplementary Material

Refer to Web version on PubMed Central for supplementary material.

## Acknowledgments

## References

1. Bos JL, Rehmann H, Wittinghofer A. GEFs and GAPs: critical elements in the control of small G proteins. Cell. 2007; 129:865–877. [PubMed: 17540168]

2. Malumbres M, Barbacid M. RAS oncogenes: the first 30 years. Nat Rev Cancer. 2003; 3:459–465. [PubMed: 12778136]

3. Vigil D, Cherfils J, Rossman KL, Der CJ. Ras superfamily GEFs and GAPs: validated and tractable targets for cancer therapy? Nat Rev Cancer. 2010; 10:842–857. [PubMed: 21102635]

4. Jemal A, et al. Cancer statistics, 2009. CA Cancer J Clin. 2009; 59:225–249. [PubMed: 19474385]

5. DiFiore F, Sesboue R, Michel P, Sabourin JC, Frebourg T. Molecular determinants of anti-EGFR sensitivity and resistance in metastatic colorectal cancer. Br J Cancer. 2010; 103:1765–1772. [PubMed: 21139621]

6. Normanno N, et al. Implications for KRAS status and EGFR-targeted therapies in metastatic CRC. Nat Rev Clin Oncol. 2009; 6:519–527. [PubMed: 19636327]

7. Wheeler DL, Dunn EF, Harari PM. Understanding resistance to EGFR inhibitors-impact on future treatment strategies. Nat Rev Clin Oncol. 2010; 7:493–507. [PubMed: 20551942]

8. Ardito CM, et al. EGF receptor is required for KRAS-induced pancreatic tumorigenesis. Cancer Cell. 2012; 22:304–317. [PubMed: 22975374]

9. Navas C, et al. EGF receptor signaling is essential for k-ras oncogene-driven pancreatic ductal adenocarcinoma. Cancer Cell. 2012; 22:318–330. [PubMed: 22975375]

10. Moore MJ, et al. Erlotinib plus gemcitabine compared with gemcitabine alone in patients with advanced pancreatic cancer: a phase III trial of the National Cancer Institute of Canada Clinical Trials Group. J Clin Oncol. 2007; 25:1960–1966. [PubMed: 17452677]

11. Aliaga JC, Deschenes C, Beaulieu JF, Calvo EL, Rivard N. Requirement of the MAP kinase cascade for cell cycle progression and differentiation of human intestinal cells. Am J Physiol. 1999; 277:G631–G641. [PubMed: 10484389]

12. Marshall CJ. Specificity of receptor tyrosine kinase signaling: transient versus sustained extracellular signal-regulated kinase activation. Cell. 1995; 80:179–185. [PubMed: 7834738]

13. Prasad A, et al. Origin of the sharp boundary that discriminates positive and negative selection of thymocytes. Proc Natl Acad Sci USA. 2009; 106:528–533. [PubMed: 19098101]

14. Das J, et al. Digital signaling and hysteresis characterize ras activation in lymphoid cells. Cell. 2009; 136:337–351. [PubMed: 19167334]

15. Ksionda O, Limnander A, Roose J. Rasgrp ras guanine nucleotide exchange factors in cancer. Front Biol. 2013; 8:508–532.

16. Kortum RL, Rouquette-Jazdanian AK, Samelson LE. Ras and extracellular signal-regulated kinase signaling in thymocytes and T cells. Trends Immunol. 2013; 34:259–268. [PubMed: 23506953]

17. Dower NA, et al. RasGRP is essential for mouse thymocyte differentiation and TCR signaling. Nat Immunol. 2000; 1:317–321. [PubMed: 11017103]

18. Kortum RL, et al. Targeted Sos1 deletion reveals its critical role in early T-cell development. Proc Natl Acad Sci USA. 2011; 108:12407–12412. [PubMed: 21746917]

19. Margarit SM, et al. Structural evidence for feedback activation by Ras. GTP of the Ras-specific nucleotide exchange factor SOS. Cell. 2003; 112:685–695. [PubMed: 12628188]

20. Boykevisch S, et al. Regulation of ras signaling dynamics by Sos-mediated positive feedback. Curr Biol. 2006; 16:2173–2179. [PubMed: 17084704]

21. Roose JP, Mollenauer M, Ho M, Kurosaki T, Weiss A. Unusual interplay of two types of Ras activators, RasGRP and SOS, establishes sensitive and robust Ras activation in lymphocytes. Mol Cell Biol. 2007; 27:2732–2745. [PubMed: 17283063]

22. Iwig JS, et al. Structural analysis of autoinhibition in the Ras-specific exchange factor RasGRP1. eLife. 2013; 2:e00813. [PubMed: 23908768]

23. Oh-hora M, Johmura S, Hashimoto A, Hikida M, Kurosaki T. Requirement for Ras guanine nucleotide releasing protein 3 in coupling phospholipase C-gamma2 to Ras in B cell receptor signaling. J Exp Med. 2003; 198:1841–1851. [PubMed: 14676298]

24. Ebinu JO, et al. RasGRP, a Ras guanyl nucleotide- releasing protein with calcium-and diacylglycerol-binding motifs. Science. 1998; 280:1082–1086. [PubMed: 9582122]

25. Cerami E, et al. The cBio cancer genomics portal: an open platform for exploring multidimensional cancer genomics data. Cancer Discov. 2012; 2:401–404. [PubMed: 22588877]

26. Reinhold WC, et al. CellMiner: a web-based suite of genomic and pharmacologic tools to explore transcript and drug patterns in the NCI-60 cell line set. Cancer Res. 2012; 72:3499–3511. [PubMed: 22802077]

27. Hartzell C, et al. Dysregulated RasGRP1 responds to cytokine receptor input in T cell leukemogenesis. Science Signaling. 2013; 6:ra21. [PubMed: 23532335]

28. van der Flier LG, Clevers H. Stem cells, self-renewal, and differentiation in the intestinal epithelium. Annu Rev Physiol. 2009; 71:241–260. [PubMed: 18808327]

29. Biteau B, Jasper H. EGF signaling regulates the proliferation of intestinal stem cells in Drosophila. Development. 2011; 138:1045–1055. [PubMed: 21307097]

30. Jiang H, Grenley MO, Bravo MJ, Blumhagen RZ, Edgar BA. EGFR/Ras/MAPK signaling mediates adult midgut epithelial homeostasis and regeneration in Drosophila. Cell Stem Cell. 2011; 8:84–95. [PubMed: 21167805]

31. Threadgill DW, et al. Targeted disruption of mouse EGF receptor: effect of genetic background on mutant phenotype. Science. 1995; 269:230–234. [PubMed: 7618084]

32. Wong VW, et al. Lrig1 controls intestinal stem-cell homeostasis by negative regulation of ErbB signalling. Nat Cell Biol. 2012; 14:401–408. [PubMed: 22388892]

33. Dieleman LA, et al. Dextran sulfate sodium-induced colitis occurs in severe combined immunodeficient mice. Gastroenterology. 1994; 107:1643–1652. [PubMed: 7958674]

34. Feng Y, et al. Mutant KRAS promotes hyperplasia and alters differentiation in the colon epithelium but does not expand the presumptive stem cell pool. Gastroenterology. 2011; 141:1003–1013. e1001–1010. [PubMed: 21699772]

35. Haigis KM, et al. Differential effects of oncogenic K-Ras and N-Ras on proliferation, differentiation and tumor progression in the colon. Nat Genet. 2008; 40:600–608. [PubMed: 18372904]

36. Bennecke M, et al. Ink4a/Arf and oncogene-induced senescence prevent tumor progression during alternative colorectal tumorigenesis. Cancer Cell. 2010; 18:135–146. [PubMed: 20708155]

37. Daley SR, et al. Rasgrp1 mutation increases naive T-cell CD44 expression and drives mTOR-dependent accumulation of Helios+ T cells and autoantibodies. eLife. 2013; 2:e01020. [PubMed: 24336796]

38. Noffsinger AE. Serrated polyps and colorectal cancer: new pathway to malignancy. Annu Rev Pathol. 2009; 4:343–364. [PubMed: 19400693]

39. Buday L, Downward J. Epidermal growth factor regulates p21ras through the formation of a complex of receptor, Grb2 adapter protein, and Sos nucleotide exchange factor. Cell. 1993; 73:611–620. [PubMed: 8490966]

40. Porfiri E, McCormick F. Regulation of epidermal growth factor receptor signaling by phosphorylation of the ras exchange factor hSOS1. J Biol Chem. 1996; 271:5871–5877. [PubMed: 8621459]

41. Kawasaki H, et al. A Rap guanine nucleotide exchange factor enriched highly in the basal ganglia. Proc Natl Acad Sci USA. 1998; 95:13278–13283. [PubMed: 9789079]

42. Jeng HH, Taylor LJ, Bar-Sagi D. Sos-mediated cross-activation of wild-type Ras by oncogenic Ras is essential for tumorigenesis. Nat Commun. 2012; 3:1168. [PubMed: 23132018]

43. Downward J, Parker P, Waterfield MD. Autophosphorylation sites on the epidermal growth factor receptor. Nature. 1984; 311:483–485. [PubMed: 6090945]

44. Topham MK, Prescott SM. Diacylglycerol kinase zeta regulates Ras activation by a novel mechanism. J Cell Biol. 2001; 152:1135–1143. [PubMed: 11257115]

45. Smith JJ, et al. Experimentally derived metastasis gene expression profile predicts recurrence and death in patients with colon cancer. Gastroenterology. 2010; 138:958–968. [PubMed: 19914252]

46. Staub E, et al. An expression module of WIPF1-coexpressed genes identifies patients with favorable prognosis in three tumor types. J Mol Med. 2009; 87:633–644. [PubMed: 19399471]

47. Jorissen RN, et al. Metastasis-associated gene expression changes predict poor outcomes in patients with Dukes stage B and C colorectal cancer. Clin Cancer Res. 2009; 15:7642–7651. [PubMed: 19996206]

48. Budczies J, et al. Cutoff Finder: a comprehensive and straightforward Web application enabling rapid biomarker cutoff optimization. PLoS ONE. 2012; 7:e51862. [PubMed: 23251644]

49. Sansom OJ, et al. Loss of Apc *in vivo* immediately perturbs Wnt signaling, differentiation, and migration. Genes Dev. 2004; 18:1385–1390. [PubMed: 15198980]

50. Moser AR, Pitot HC, Dove WF. A dominant mutation that predisposes to multiple intestinal neoplasia in the mouse. Science. 1990; 247:322–324. [PubMed: 2296722]

51. Su LK, et al. Multiple intestinal neoplasia caused by a mutation in the murine homolog of the APC gene. Science. 1992; 256:668–670. [PubMed: 1350108]

52. Taketo MM, Edelmann W. Mouse models of colon cancer. Gastroenterology. 2009; 136:780–798. [PubMed: 19263594]

53. Lee D, et al. Tumor-specific apoptosis caused by deletion of the ERBB3 pseudo-kinase in mouse intestinal epithelium. J Clin Invest. 2009; 119:2702–2713. [PubMed: 19690388]

54. Roberts RB, et al. Importance of epidermal growth factor receptor signaling in establishment of adenomas and maintenance of carcinomas during intestinal tumorigenesis. Proc Natl Acad Sci USA. 2002; 99:1521–1526. [PubMed: 11818567]

55. Yang D, et al. RasGRP3, a Ras activator, contributes to signaling and the tumorigenic phenotype in human melanoma. Oncogene. 2011

56. Yang D, et al. RasGRP3 contributes to formation and maintenance of the prostate cancer phenotype. Cancer Res. 2010; 70:7905–7917. [PubMed: 20876802]

57. Oki-Idouchi CE, Lorenzo PS. Transgenic overexpression of RasGRP1 in mouse epidermis results in spontaneous tumors of the skin. Cancer Res. 2007; 67:276–280. [PubMed: 17210708]

58. Ahmed Z, et al. Grb2 controls phosphorylation of FGFR2 by inhibiting receptor kinase and Shp2 phosphatase activity. J Cell Biol. 2013; 200:493–504. [PubMed: 23420874]

59. Lin CC, et al. Inhibition of basal FGF receptor signaling by dimeric Grb2. Cell. 2012; 149:1514–1524. [PubMed: 22726438]

60. Wang Z, Wang M, Lazo JS, Carr BI. Identification of epidermal growth factor receptor as a target of Cdc25A protein phosphatase. J Biol Chem. 2002; 277:19470–19475. [PubMed: 11912208]

61. Prahallad A, et al. Unresponsiveness of colon cancer to BRAF(V600E) inhibition through feedback activation of EGFR. Nature. 2012; 483:100–103. [PubMed: 22281684]

62. Diaz LA Jr, et al. The molecular evolution of acquired resistance to targeted EGFR blockade in colorectal cancers. Nature. 2012; 486:537–540. [PubMed: 22722843]

63. Misale S, et al. Emergence of KRAS mutations and acquired resistance to anti-EGFR therapy in colorectal cancer. Nature. 2012; 486:532–536. [PubMed: 22722830]

64. Barretina J, et al. The Cancer Cell Line Encyclopedia enables predictive modelling of anticancer drug sensitivity. Nature. 2012; 483:603–607. [PubMed: 22460905]

65. The Cancer Genome Atlas Network. Comprehensive molecular characterization of human colon and rectal cancer. Nature. 2012; 487:330–337. [PubMed: 22810696]

66. Nishiyama Y, Kataoka T, Yamato K, Taguchi T, Yamaoka K. Suppression of dextran sulfate sodium-induced colitis in mice by radon inhalation. Mediators Inflamm. 2012; 2012:239617. [PubMed: 23365486]

67. Rhodes DR, et al. ONCOMINE: a cancer microarray database and integrated data-mining platform. Neoplasia. 2004; 6:1–6. [PubMed: 15068665]

68. Edgar R, Domrachev M, Lash AE. Gene Expression Omnibus: NCBI gene expression and hybridization array data repository. Nucleic Acids Res. 2002; 30:207–210. [PubMed: 11752295]

69. Sato T, et al. Single Lgr5 stem cells build crypt-villus structures *in vitro* without a mesenchymal niche. Nature. 2009; 459:262–265. [PubMed: 19329995]
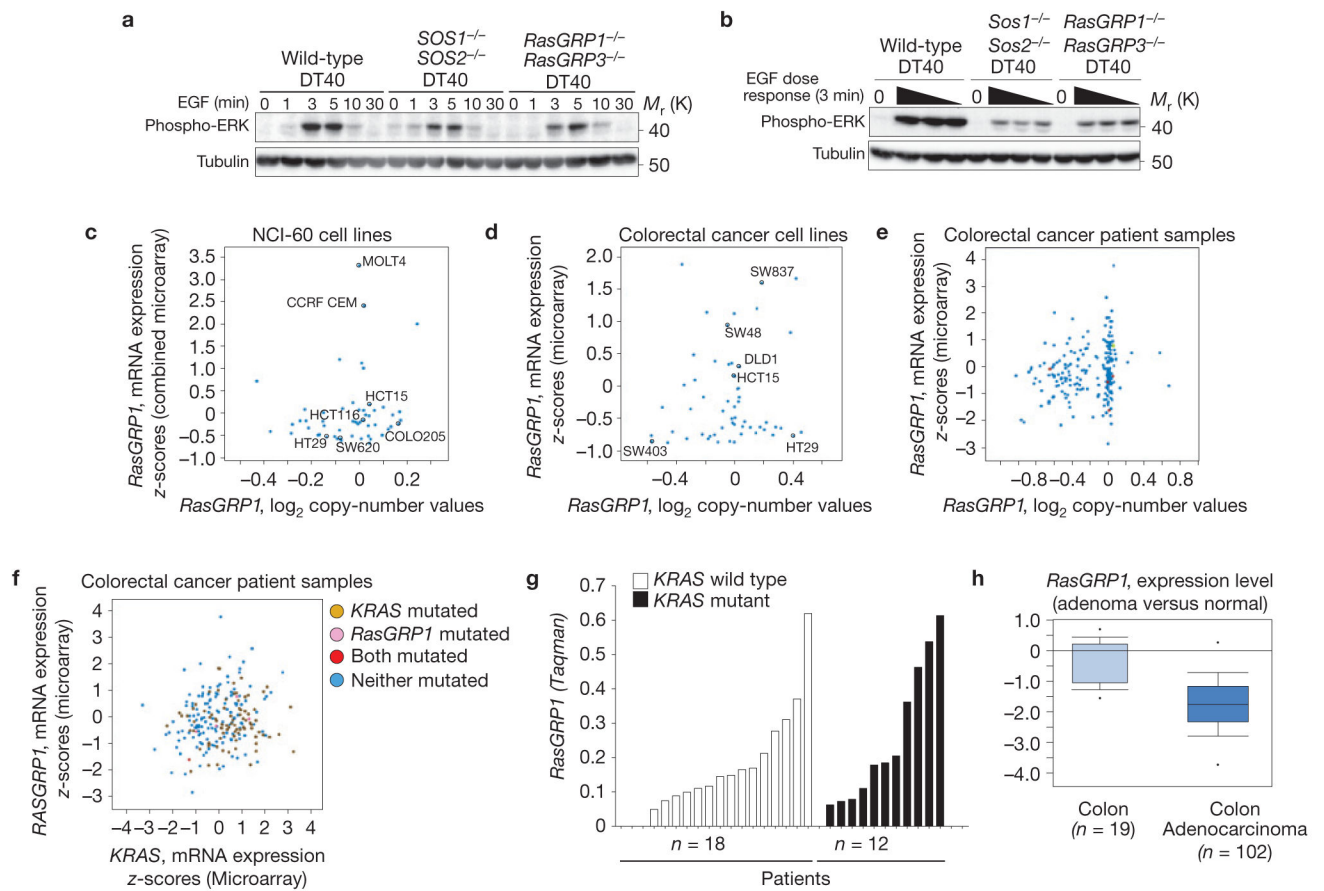
**Figure 1.**

RasGRP1 is expressed in CRC cell lines and CRC patient tumour samples. (**a**) Time course of EGF-induced ERK phosphorylation in DT40 B cells that are WT or genetically deleted for SOS1 and SOS2, or for RasGRP1 and RasGRP3. EGF dose is 10 ng ml$^{-1}$. Tubulin serves as protein loading control. (**b**) As in **a**, but analysing the effects of 25, 5 and 1 ng ml$^{-1}$ EGF in a 3 min stimulation. Panels **a,b** are representative results of 3 or more independent experiments. Unprocessed original scans of western blots are shown in Supplementary Fig. 7. (**c**) Plots showing *RasGRP1* mRNA expression *z*-scores versus copy number value in NCI-60 cell lines[26] were obtained through cBioPortal[25]. Each blue dot represents one cell line. Some CRC cell lines and leukaemia cell lines are noted for reference. (**d**) Plots showing *RasGRP1* mRNA expression *z*-scores versus copy number value in 56 CRC cell lines[25,64]. Various CRC cell lines used in our study are noted on the plot. (**e**) *RasGRP1* mRNA expression *z*-scores versus copy number value in human colon cancer patients (*n* = 276) from the TCGA Colorectal Adenocarcinoma data set[25,65]. Each dot represents a sample with no mutation on RasGRP1 (blue), missense mutation (red, *n*= 5) or nonsense (yellow). (**f**) *RasGRP1* mRNA expression *z*-scores plotted against KRAS mRNA expression *z*-scores for the 276 patient samples in **e**. Colours represent mutational status[25]. (**g**) *RasGRP1* mRNA expression determined by Taqman PCR on liver metastases samples surgically removed from 30 CRC patients. (**h**) Oncomine analysis was performed to examine *RASGRP1* expression in human colon adenocarcinoma and normal colon using

online TCGA microarray data. *RASGRP1* levels are decreased in colon adenocarcinoma compared with normal tissues. Results are shown as box plots representing the median, 25th and 75th percentiles as boxes, as well as 10th and 90th percentiles as bars, using GraphPad Prism. *RASGRP1* levels in colon adenocarcinoma ($n$= 102, maxima, 0.318; minima, −3.766) are decreased (fold change, −2.244; $P = 6.73 \times 10^{-10}$ (Student's *t*-test)) compared with normal tissue ($n$= 19, maxima, 0.794; minima, −1.582).
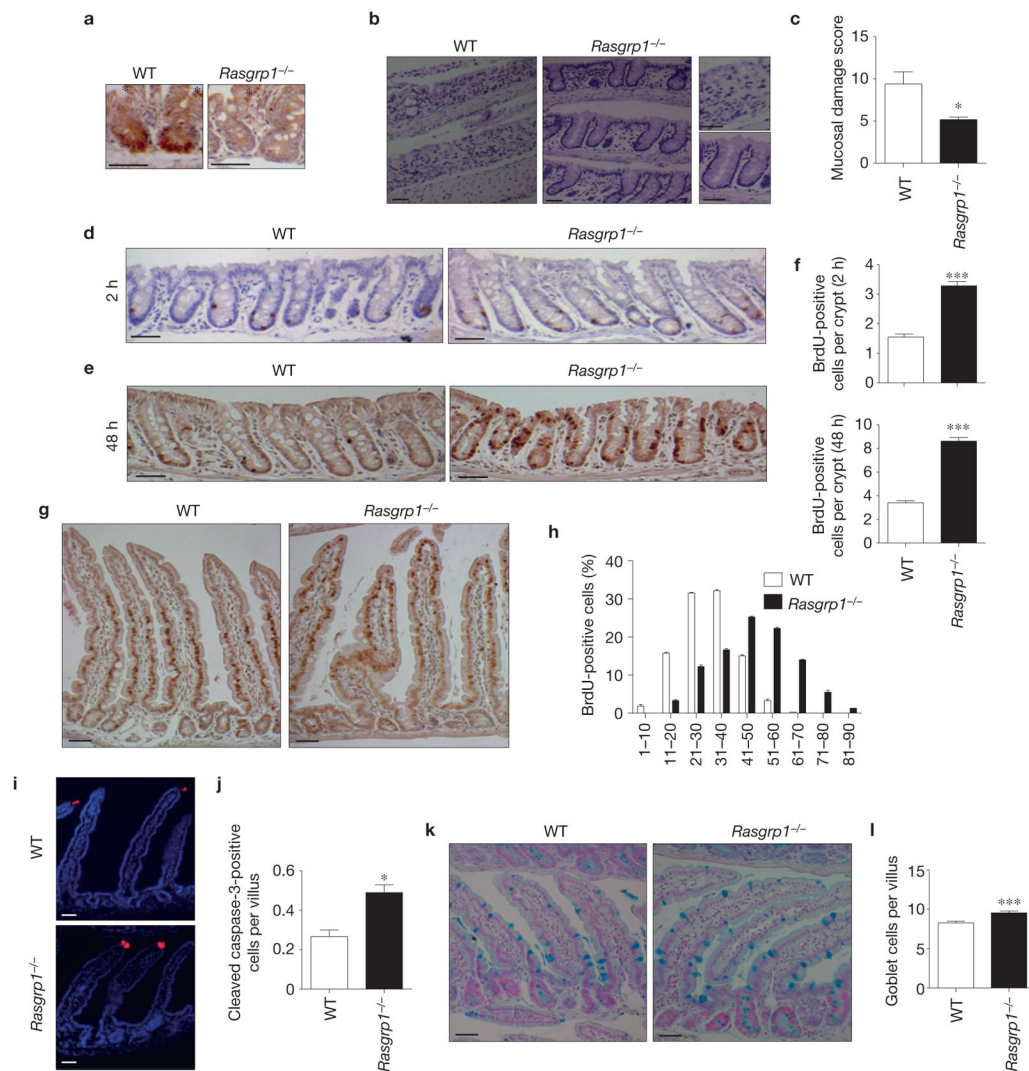
**Figure 2.**

Rasgrp1 plays a role in intestinal epithelial cell proliferation and goblet cell generation. (**a**) Immunohistochemistry for Rasgrp1 protein (brown) in the small intestines of WT and *Rasgrp1*$^{-/-}$ mice. The asterisks denote nonspecific staining observed in both mouse models. Scale bars, 150 μm. (**b**) *Rasgrp1*-deficient mice demonstrate resistance to DSS-induced colitis. Representative images of WT and *Rasgrp1*$^{-/-}$ mice at 5 days of DSS treatment. (**c**) Analysis of mucosal damage following 5 days of DSS treatment. Scores ranging from 0 to 12 were obtained by combining three parameters, as published[66]. Data are depicted as bar graphs with mean score ± s.e.m. obtained from *n*= 5 mice for WT and *n*= 6 mice for *Rasgrp1*$^{-/-}$. *$P$ = 0.0115 (unpaired *t*-test). (**d,e**) Representative images of short- (2 h, **d**) and long-term (48 h, **e**) *in vivo* BrdU-labelling assays in the colon of WT or *Rasgrp1*$^{-/-}$ mice. Scale bars, 100 μm. (**f**) Quantification and statistical analysis of BrdU-positive cells in the colon. *n*= 150 crypts pooled from 3 WT mice and *n*= 150 crypts pooled from 3 *Rasgrp1*$^{-/-}$ mice were counted to obtain mean ± s.e.m. ***$P$ < 0.0001 (Wilcoxon matched-pairs signed rank test). (**g**) Long-term (48 h) *in vivo* BrdU labelling in the small intestine. Scale bars, 100

μm. (**h**) Positioning of BrdU-positive cells in the small intestine. $n = 120$ crypt–villus axes pooled from 3 WT mice and $n = 120$ pooled from 3 *Rasgrp1*$^{-/-}$ mice were counted. Data are represented as percentage of cells per position ± s.e.m. (**i**) Representative images of small intestines of WT- and *Rasgrp1*$^{-/-}$ mice stained for cleaved caspase-3 (red) and DAPI (blue). Scale bars, 100 μm. (**j**) Quantification of cleaved caspase-3-positive cells in the small intestine from mice with the indicated genotype. $n = 360$ transversally sectioned villi pooled from 3 WT mice and $n = 360$ pooled from *Rasgrp1*$^{-/-}$ mice were counted to obtain the mean ± s.e.m. graphed as positive cells per villus. $^*P < 0.05$ (unpaired *t*-test). (**k,l**) Alcian blue staining (**k**) to visualize goblet cell presence in the small intestine (duodenum). Scale bars, 100 μm. (**l**) Data represent mean ± s.e.m. $n = 150$ transversally sectioned villi pooled from 3 WT mice and $n = 150$ pooled from 3 *Rasgrp1*$^{-/-}$ mice were counted. $^{***}P < 0.001$ (Wilcoxon *t*-test).
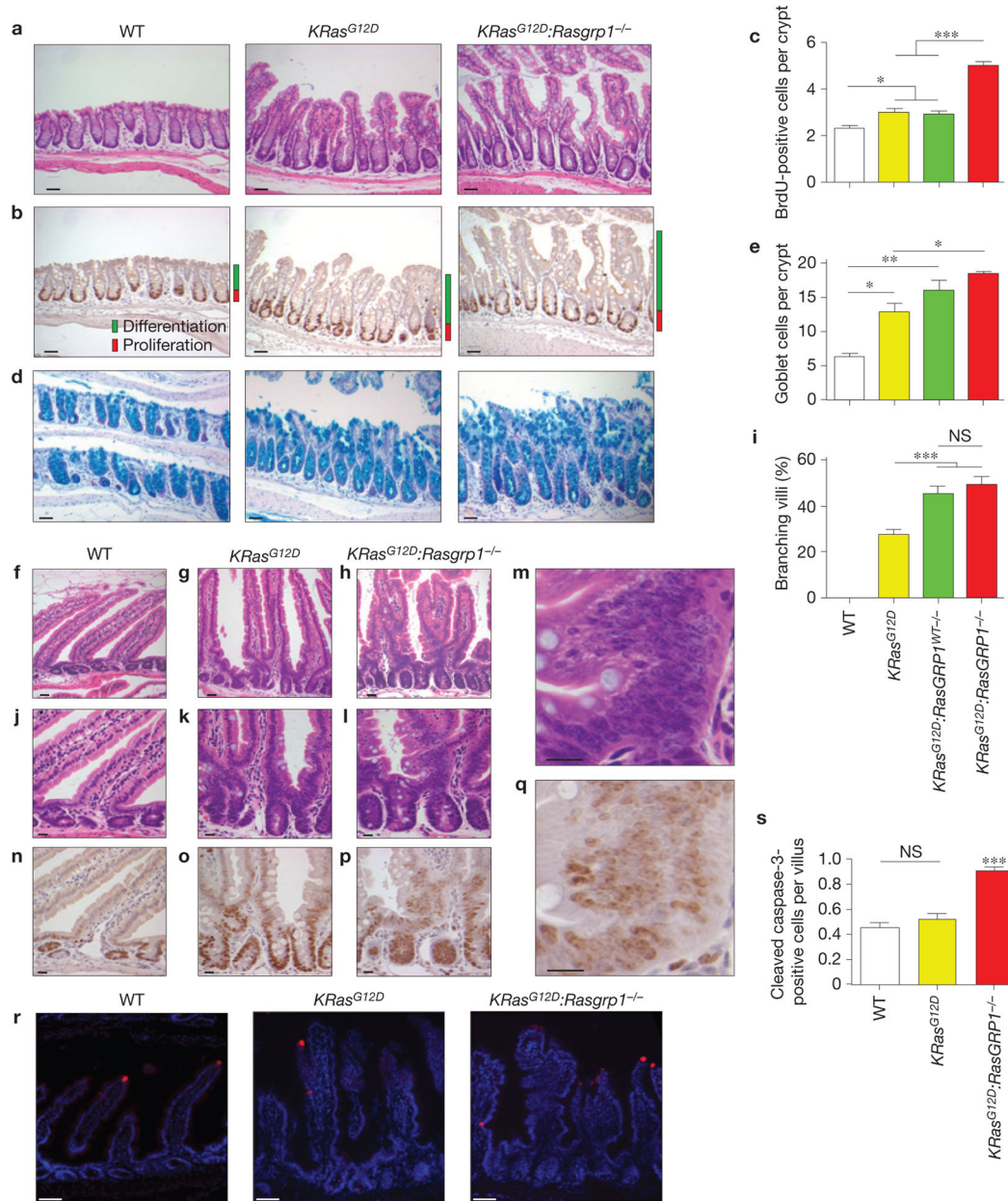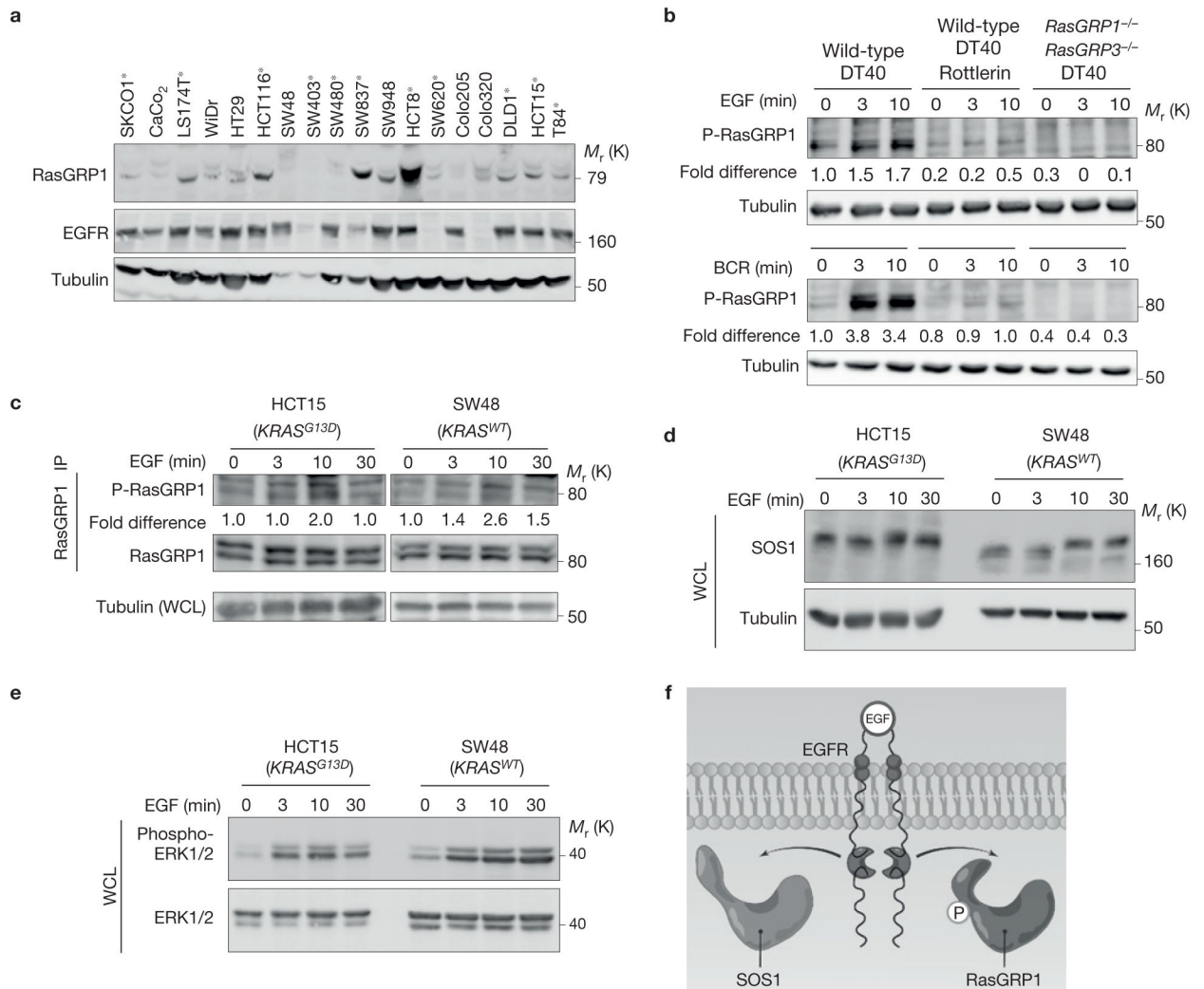
**Figure 3.**

Loss of one or two *Rasgrp1* alleles exacerbates serrated dysplasia of *KRas*^G12D^ epithelium. (**a**,**b**) Representative sections of colon with haematoxylin & eosin (H&E; **a**) or Ki67 staining (**b**), revealing the serrated dysplasia of the colonic epithelium in *KRas*^G12D^ mice that is further exacerbated with loss of Rasgrp1. Scale bars, 50 μm. See also Supplementary Figs 1 and 2. (**c**) Quantification of diving cells in crypt regions of the colon following a short-term (2 h) *in vivo* BrdU-labelling assay. Data are mean ± s.e.m. *n* = 150 open crypts pooled from 3 mice were counted for each genotype. *$P < 0.05$, ***$P < 0.0001$ (one-way ANOVA, Bonferroni's multiple comparison test). (**d**) Representative images of colonic sections with Alcian blue staining to reveal goblet cells. Scale bars, 50 μm. (**e**) Quantification of goblet

cells in the distal colon. Goblet cells in $n=$ 150 open crypts pooled from 3 mice were counted for each genotype to obtain the graphed mean ± s.e.m. $^*P < 0.05$, $^{**}P < 0.001$ (one-way ANOVA, Bonferroni's). (**f**–**h**) Representative H&E-stained sections of small intestine demonstrating the branched villi in $KRas^{G12D}$ and $KRas^{G12D}:Rasgrp1^{-/-}$ mice. Scale bars, 50 μm. See also Supplementary Fig. 2 where purposely distinct, representative fields from the small intestine are shown. (**i**) Quantification of branching villi in the small intestine. Data are plotted as mean ± s.e.m. pooled from 3 mice for each genotype ($KRas^{G12D}$ $n = 120$ total villi; $KRas^{G12D}:Rasgrp1^{WT/-}$ $n = 141$; and $KRas^{G12D}:Rasgrp1^{-/-}$ $n = 148$). $^{***}P < 0.0001$ (one-way ANOVA, Bonferroni's). No branching is observed in WT mice. (**j**–**q**) Higher magnifications of branching villi (**j**–**l**) with Ki67 staining (**n**–**p**). Scale bars, 100 μm. (**m**,**q**) Detail of the aberrant transit-amplifying (T/A) zone in $KRas^{G12D}:Rasgrp1^{-/-}$ small intestine (from **l**,**p**). (**r**) Representative images of the small intestine sections stained for cleaved caspase-3 (red) and DAPI (blue) from control WT-, $KRas^{G12D}$- and $KRas^{G12D}:Rasgrp1^{-/-}$ mice. Scale bars, 100 μm. (**s**) Quantification of cleaved caspase-3-positive cells in the small intestine. Data are percentage of positive cells ± s.e.m. obtained from 4 pooled mice per genotype (WT, $n = 270$; $KRas^{G12D}$, $n = 253$; $KRas^{G12D}:Rasgrp1^{-/-}$, $n = 278$). NS, not significant; $^{***}P < 0.0001$ (one-way ANOVA, Bonferroni's).

**Figure 4.**
EGFR connects to both RasGRP1 and SOS1. (**a**) Detection of RasGRP1 and EGFR
expression by western blot in 18 CRC cell lines. Asterisks indicate *KRAS* mutations
(*KRAS^MUT^*). See also Supplementary Table 1. (**b**) RasGRP1 phosphorylation in EGF- or
BCR-stimulated DT40 B cells. PKC inhibitor (rottlerin) and genetic deletion of RasGRP1/3
function as specificity controls and tubulin as a protein loading control. (**c**) Detection of
RasGRP1 phosphorylation in EGF-stimulated HCT15 and SW48 CRC cells from which
RasGRP1 protein was immunoprecipitated (IP). Blotting for total RasGRP1 levels reveals
equal efficiency of the IP and tubulin expression of whole-cell lysates (WCL) demonstrates
equal protein input for the IP. (**d,e**) Detection of EGF-induced SOS1 mobility shifts and
ERK phosphorylation in WCL of HCT15 and SW48 cells. All panels are representative
results of three or more independent experiments. Unprocessed original scans of western
blots are shown in Supplementary Fig. 7. (**f**) Cartoon of EGFR–RasGRP1 and EGFR–SOS1
signalling.
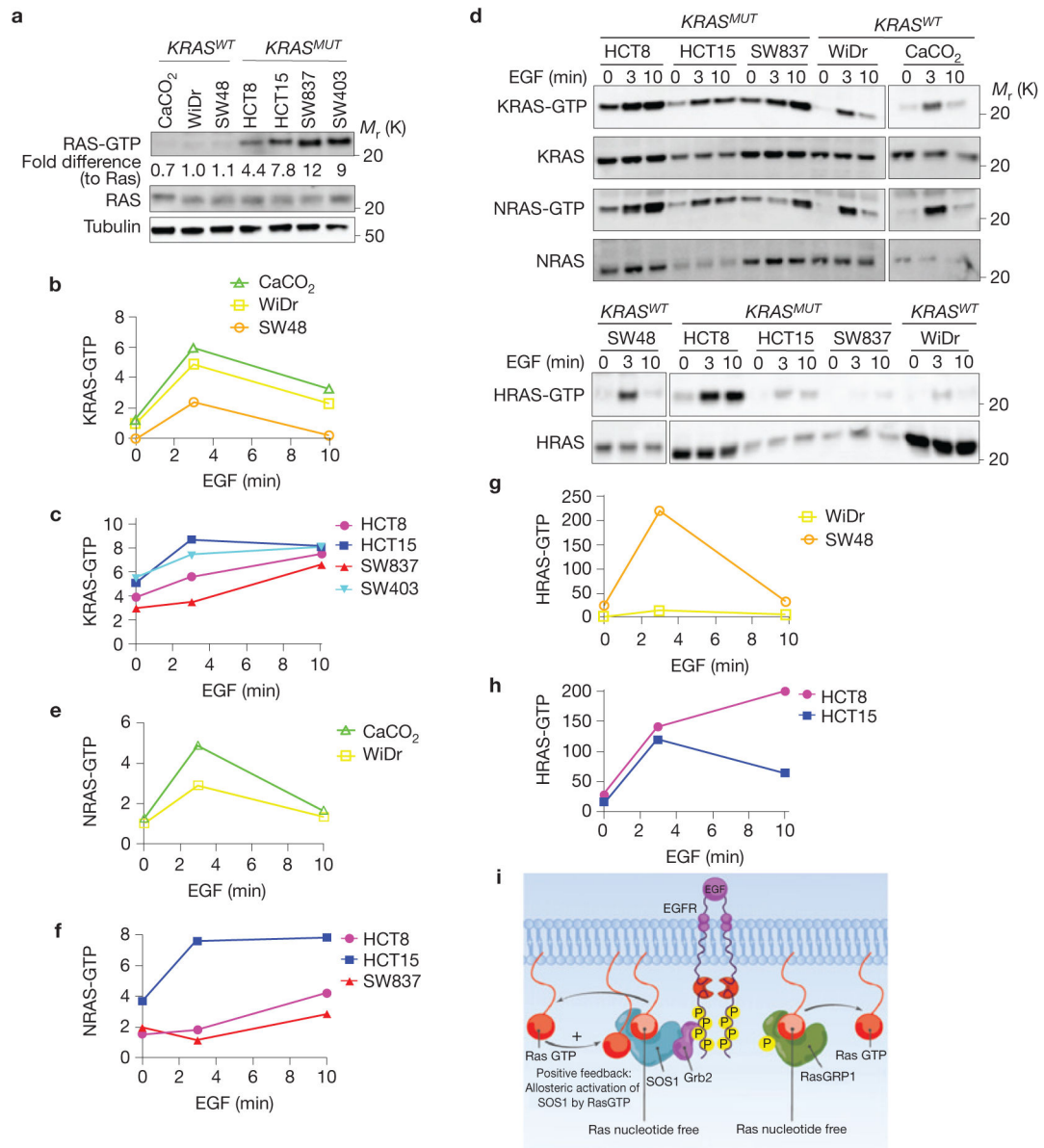
**Figure 5.**
Hyperactivation of RAS in EGF-stimulated $KRAS^{MUT}$ CRC cells. (**a**) Total baseline RAS–GTP levels in serum-starved CRC cells. Levels are normalized to RAS and arbitrarily set at 1.0 in WiDr cells. (**b,c**) KRAS–GTP profile of time courses with EGF-stimulated (5 ng ml$^{-1}$) KRAS WT cells ($KRAS^{WT}$) (**b**) and KRAS mutant cells ($KRAS^{MUT}$) (**c**). (**d**) Representative examples of pulldown assays on the indicated RAS–GTP isoforms in different CRC cell lines after starvation and EGF (5 ng ml$^{-1}$) stimulation. Specific RAS proteins were detected by western blot using H-, N- or KRAS-specific antibodies. (**e–h**) Quantification of N- and HRAS activation in the indicated cell lines as in **b,c**. (**i**) Cartoon of Grb2-SOS1 recruitment to tyrosine-phosphorylated EGFR and allosteric activation of SOS1 through a positive feedback loop by Ras–GTP. All data are representative examples of three
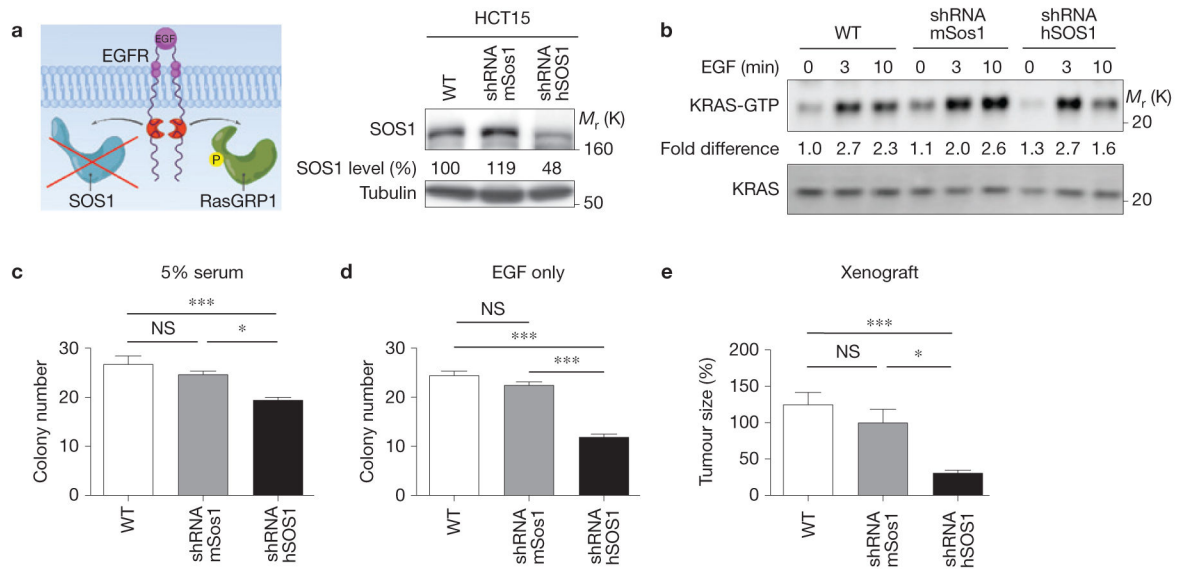
or more independent experiments and unprocessed original scans of western blots are shown in Supplementary Fig. 7.

**Figure 6.**
EGFR–SOS1 signals promote EGFR–Ras signalling and tumorigenesis of *KRAS^{MUT}* CRC cells. (**a**) Detection of SOS1 expression in HCT15 cells with knockdown for human SOS1 (shRNA hSOS1). shRNA for murine Sos1 (shRNA mSOS1) is used as a specificity control. (**b**) Detection of KRAS-GTP in the indicated EGF-stimulated ($5 \text{ ng ml}^{-1}$) HCT15 cell populations. KRAS-GTP levels are quantified and corrected for by total KRAS levels. Unstimulated WT HCT15 cells are arbitrarily set at 1.0. Representative results of four independent experiments. Unprocessed original scans of western blots are shown in Supplementary Fig. 7. (**c,d**) Soft-agar colony formation assays of the indicated HCT15 cell populations that were grown in growth medium with 5% serum (**c**) or in serum-free medium supplemented with $10 \text{ ng ml}^{-1}$ EGF (**d**). Fifteen fields pooled from 3 independent experiments were counted per condition (WT, $n = 15$; shRNA mSos1, $n = 15$; shRNA hSOS1, $n = 15$). Data are mean ± s.e.m. NS, not significant; $^{*}P < 0.05$, $^{***}P < 0.0001$ (one-way ANOVA, Bonferroni's multiple comparison test). (**e**) Relative tumour size of the indicated HCT15 cells xenografted into nude mice and measured 40 days after injection. WT, $n = 7$ mice; shRNA mSos1, $n = 9$; shRNA hSOS1, $n = 10$, all pooled from 2 independent experiments. Results are given as percentages with one WT arbitrarily set at 100%. Means with standard errors (±s.e.m.) are plotted. NS, not significant; $^{*}P < 0.05$, $^{***}P < 0.0001$ (unpaired *t*-test).
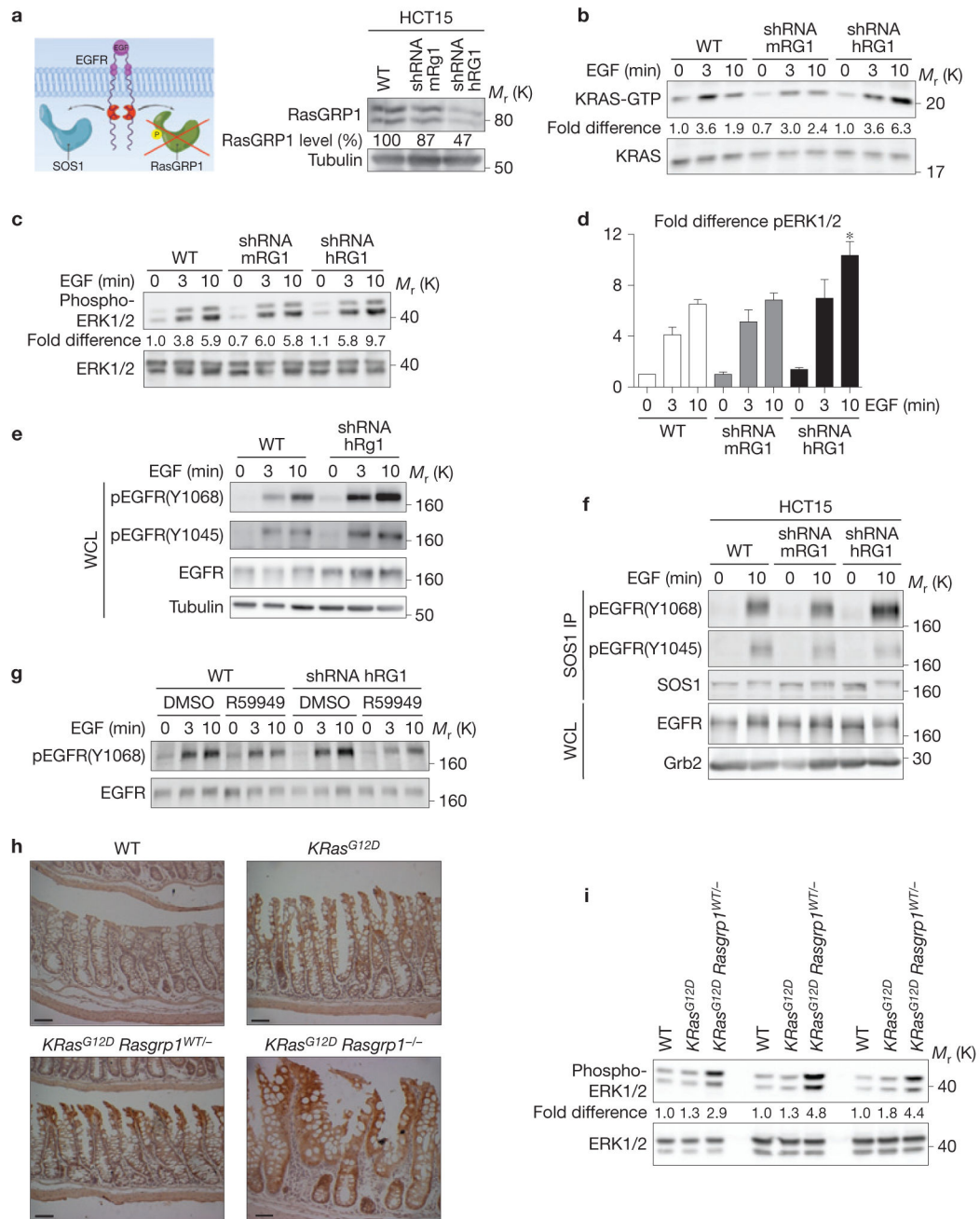
**Figure 7.**

RasGRP1 feedback restricts EGFR–SOS1–Ras signals. (**a**) Detection of RasGRP1 expression in $KRAS^{MUT}$ HCT15 cells analogous to Fig. 6a. Knockdown for murine Rasgrp1 (shRNA mRg1) functions as a control. (**b**) KRAS-GTP levels in the indicated EGF-stimulated (5 ng ml$^{-1}$) HCT15 cell populations. Note the increase in KRAS-GTP levels at the 10-min time point when RasGRP1 expression levels are reduced. (**c**) Analysis of ERK phosphorylation and total ERK protein levels in the same cell lysates presented in **b**. Unstimulated WT HCT15 cells are arbitrarily set at 1.0. (**d**) Quantification of ERK phosphorylation. Data are plotted as fold difference ± s.e.m. $n = 3$ independent experimental

sets (**c** and Supplementary Fig. 4a,b). $^*P < 0.05$ (one-way ANOVA, Bonferroni's) comparing the 10-min time point of shRNA hRG1 with that for WT and shRNA mRG1. (**e**) Analysis of EGFR phosphorylation in WCL of EGF-stimulated (25 ng ml$^{-1}$) cells. (**f**) Analysis of EGF-induced complexes of Grb2–SOS1 with P-Y$_{1068}$-EGFR. SOS1 was immunoprecipitated (SOS1 IP) from the indicated HCT15 cells and immunoprecipitates were blotted with specific antibodies against the indicated proteins. Note the increased levels of P-Y$_{1068}$-EGFR that immunoprecipitated with SOS1 in an EGF-stimulatory-dependent manner when RasGRP1 levels are reduced. (**g**) Analysis of P-Y$_{1068}$-EGFR in the indicated EGF-stimulated HCT15 populations as in **e**. Cells were treated with R59949 DGK inhibitor to enhance DAG-RasGRP1 signalling or with dimethylsulphoxide (DMSO) as a control. R59949 exposure results in decreased levels of P-Y$_{1068}$-EGFR. All western blot panels in Fig. 7 are representative of three or more independent experiments and unprocessed original scans of western blots are shown in Supplementary Fig. 7. (**h**) Immunohistochemical analysis of ERK phosphorylation levels in brown staining in the colonic epithelium of the indicated mouse genotypes. Images of distal colonic epithelium are representative results of two mice per genotype. Scale bars, 100 μm. (**i**) Analysis of ERK phosphorylation and total ERK protein level of mouse intestinal epithelial cells (IEC) isolated from colon of control WT, *KRas$^{G12D}$*, *KRas$^{G12D}$ Rasgrp1$^{WT/-}$* mice (6 months old). Blots show three independent experiments. P-ERK in IEC from WT mice is arbitrarily set at 1.0 for each experiment.
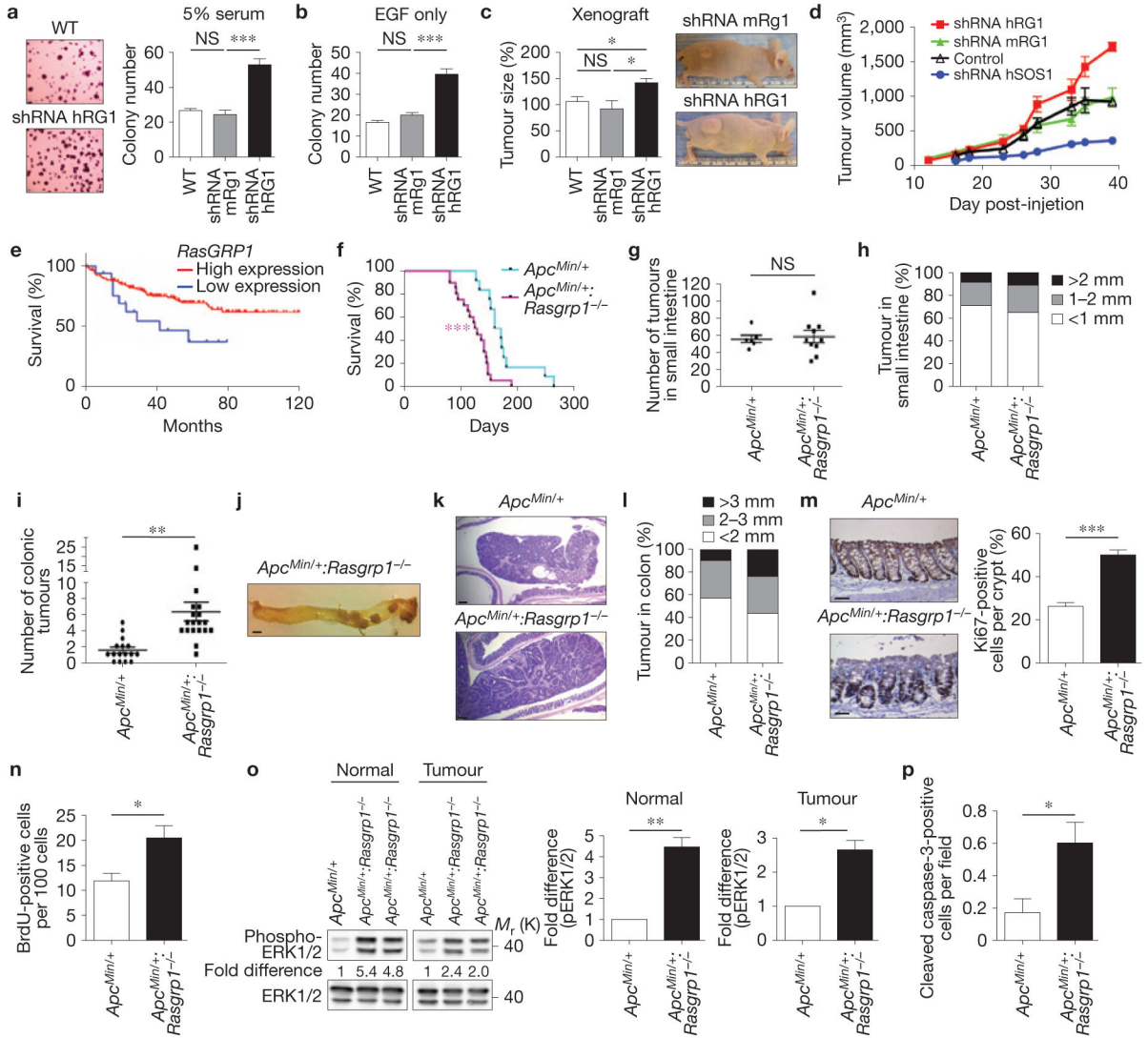
**Figure 8.**

RasGRP1 limits CRC cell proliferation and *in vivo* tumour growth. (**a,b**) Reduction of RasGRP1 expression by 53% results in increased growth in soft-agar colony formation assays. Quantification and analysis as in Fig. 6c. NS, not significant; [***]$P < 0.0001$ (one-way ANOVA, Bonferroni's multiple comparison test). $n = 15$ fields pooled from 3 independent experiments were counted per condition (WT, $n = 15$; shRNA mSos1, $n = 15$; shRNA hSOS1, $n= 15$). Data are mean ± s.e.m. (**c**) Xenografted HCT15 cells were analysed as in Fig. 6e. WT, $n= 9$ mice; shRNA mRg1, $n= 10$; shRNA hRG1, $n= 10$; all pooled from 2 independent experiments. [*]$P < 0.05$ (unpaired *t*-test). (**d**) Growth rates of the indicated xenografted HCT15 cells. Specifics of HCT15 cells with shRNA hSOS1 are inserted in blue for comparison. Data are mean ± s.e.m. WT, $n = 3$; shRNA mRg1, $n = 3$; shRNA hRG1, $n= 4$; shRNA hSOS1, $n= 4$. (**e**) Kaplan–Meier survival curve for 172 patient samples with high *RasGRP1* expression level (red line; $n= 155$ patients) and low *RasGRP1* expression level (blue line; $n= 17$ patients) ($P = 0.0243$, log-rank (Mantel–Cox) Test). Similar results were obtained with two independent studies[46,47] (see Supplementary Fig. 5a,b). (**f**) Kaplan–Meier

survival curve showing decreased survival of $Apc^{Min/+}$ mice deleted for *Rasgrp1* ($n = 20$) compared with $Apc^{Min/+}$ mice ($n = 12$). [***]$P < 0.0006$, log-rank (Mantel–Cox) test. (**g**) Quantification of numbers of tumours in small intestine of $Apc^{Min/+}$ ($n = 6$) and $Apc^{Min/+}:Rasgrp1^{-/-}$ ($n = 10$) mice. NS, not significant. Data are plotted with the mean as a horizontal line and s.e.m. as error bars. (**h**) Tumour sizes in small intestines of $Apc^{Min/+}$ and $Apc^{Min/+}:Rasgrp1^{-/-}$ mice. Results are depicted as percentage of tumours falling into three size categories pooled from $n = 6$ $Apc^{Min/+}$ mice and 337 tumours; $n = 10$ $Apc^{Min/+}:Rasgrp1^{-/-}$ mice and 588 tumours. (**i**) Quantification of colonic tumour incidence in $Apc^{Min/+}$ and $Apc^{Min/+}:Rasgrp1^{-/-}$ mice ($n = 16$ and 19 mice respectively; data are plotted as mean ± s.e.m. [**]$P < 0.01$ (unpaired *t*-test)). (**j**) Representative image of a $Apc^{Min/+}:Rasgrp1^{-/-}$ colon. Scale bar, 5 mm. (**k**) Representative H&E images from colonic tumours from $Apc^{Min/+}$ and $Apc^{Min/+}:Rasgrp1^{-/-}$ mice. Scale bars, 150 μm. (**l**) Bar graph of colonic tumour size analysis for $Apc^{Min/+}$ and $Apc^{Min/+}:Rasgrp1^{-/-}$ mice. $n = 10$ $Apc^{Min/+}$ mice and 21 tumours; $n = 19$ $Apc^{Min/+}:Rasgrp1^{-/-}$ mice and 123 tumours. (**m**) Representative colon sections stained for Ki67 in crypts of $Apc^{Min/+}$ and $Apc^{Min/+}:Rasgrp1^{-/-}$ mice. Scale bars, 100 μm. $n = 60$ open crypts pooled from 3 $Apc^{Min/+}$ mice and $n = 80$ crypts pooled from 4 $Apc^{Min/+}:Rasgrp1^{-/-}$ mice were counted and depicted as percentage of Ki67-positive cells with standard errors (± s.e.m.). [***]$P < 0.0001$, (unpaired *t*-test). (**n**) Quantification of BrdU-positive cells in colonic tumours. Three to six square fields (100 μm × 100 μm) were randomly selected in tumours from $Apc^{Min/+}$ ($n = 3$) and $Apc^{Min/+}:Rasgrp1^{-/-}$ ($n = 3$) mice and BrdU-positive cells were enumerated. $n = 16$ fields from 5 tumours for $Apc^{Min/+}$ and $n = 37$ fields from 7 tumours for $Apc^{Min/+}:Rasgrp1^{-/-}$ were counted. Data represent mean ± s.e.m., [*]$P < 0.05$ (unpaired *t*-test). (**o**) Representative ERK phosphorylation and total ERK protein levels of normal colon and colonic tumours. P-ERK in $Apc^{Min/+}$ mice is arbitrarily set at 1.0 for each experiment. Data are mean of fold difference ± s.e.m. $n = 5$ protein extractions per mouse genotype. [*]$P < 0.05$, [**]$P < 0.01$ (paired *t*-test). (**p**) Quantification of cleaved caspase-3-positive cells obtained as in **n**. Data are percentage of positive cells ± s.e.m. $n = 16$ fields from 5 tumours for $Apc^{Min/+}$ and $n = 37$ fields from 7 tumours for $Apc^{Min/+}:Rasgrp1^{-/-}$ were counted. [*]$P < 0.05$ (unpaired *t*-test). Unprocessed original scans of blots are shown in Supplementary Fig. 7.